

# Kinetic freeze-out temperatures in central and peripheral collisions: Which one is larger?

Hai-Ling Lao, Fu-Hu Liu\*, Bao-Chun Li, Mai-Ying Duan

*Institute of Theoretical Physics & State Key Laboratory of Quantum Optics and Quantum Optics Devices,  
Shanxi University, Taiyuan, Shanxi 030006, China*

**Abstract:** The kinetic freeze-out temperatures,  $T_0$ , in nucleus-nucleus collisions at the Relativistic Heavy Ion Collider (RHIC) and Large Hadron Collider (LHC) energies are extracted by four methods: i) the Blast-Wave model with Boltzmann-Gibbs statistics (the BGBW model), ii) the Blast-Wave model with Tsallis statistics (the TBW model), iii) the Tsallis distribution with flow effect (the improved Tsallis distribution), and iv) the intercept in  $T = T_0 + am_0$  (the alternative method), where  $m_0$  denotes the rest mass and  $T$  denotes the effective temperature which can be obtained by different distribution functions. It is found that the relative sizes of  $T_0$  in central and peripheral collisions obtained by the conventional BGBW model which uses a zero or nearly zero transverse flow velocity,  $\beta_T$ , are contradictory in tendency with other methods. With a re-examination for  $\beta_T$  in the first method in which  $\beta_T$  is taken to be  $\sim (0.40 \pm 0.07)c$ , a recalculation presents a consistent result with others. Finally, our results show that the kinetic freeze-out temperature in central collisions is larger than that in peripheral collisions.

**Keywords:** kinetic freeze-out temperature, methods for extraction, central collisions, peripheral collisions

**PACS:** 25.75.Ag, 25.75.Dw, 24.10.Pa

## 1 Introduction

Temperature is an important concept in high energy nucleus-nucleus collisions. Usually, three types of temperatures which contain the chemical freeze-out temperature, kinetic freeze-out temperature, and effective temperature are used in literature [1–5]. The chemical freeze-out temperature describes the excitation degree of the interacting system at the stage of chemical equilibrium in which the chemical components (relative fractions) of particles are fixed. The kinetic freeze-out temperature describes the excitation degree of the interacting system at the stage of kinetic and thermal equilibrium in which the (transverse) momentum spectra of particles are no longer changed. The effective temperature is not a real temperature. In fact, the effective temperature is related to particle mass and can be extracted from the transverse momentum spectra by using some distribution laws such as the standard (Boltzmann, Fermi-Dirac, and Bose-Einstein), Tsallis, and so forth.

Generally, the chemical freeze-out temperature is usually obtained from the particle ratios [6–8]. It is equal to or larger than the kinetic freeze-out tempera-

ture due to the the chemical equilibrium being meanwhile or earlier than the kinetic equilibrium. The effective temperature is larger than the kinetic freeze-out temperature due to mass and flow effects [9, 10]. Both the chemical freeze-out and effective temperatures in central nucleus-nucleus collisions are larger than those in peripheral collisions due to more violent interactions occurring in central collisions. In fact, central collisions contain more nucleons, and peripheral collisions contains less nucleons. Usually, there are small dissents in the extractions of chemical freeze-out temperature and effective temperature. As for the extraction of kinetic freeze-out temperature, the situations are largely non-uniform.

Currently, four main methods are used in the extraction of kinetic freeze-out temperature  $T_0$ , which are i) the Blast-Wave model with Boltzmann-Gibbs statistics (the BGBW model) [11–13], ii) the Blast-Wave model with Tsallis statistics (the TBW model) [14], iii) the Tsallis distribution with flow effect (the improved Tsallis distribution) [15, 16], and iv) the intercept in  $T = T_0 + am_0$  (the alternative method) [12, 17–20], where  $m_0$  denotes the rest mass and  $T$  denotes the effective temperature which can be obtained by different

\*E-mail: fuhuliu@163.com; fuhuliu@sxu.edu.cn

distribution functions. In detail, the alternative method can be divided into a few sub-methods due to different distributions being used. Generally, we are inclined to use the standard and Tsallis distributions in the alternative method due to the standard distribution being closest to the ideal gas model in thermodynamics, and the Tsallis distribution describing a wide spectrum which needs two- or three-component standard distribution to be fitted [21].

The kinetic freeze-out temperature  $T_0$  and the mean transverse radial flow velocity  $\beta_T$  can be simultaneously extracted by the first three methods. The alternative method needs further treatments in extracting the flow velocity. In our recent works [22–24], the mean transverse flow velocity  $\beta_T$  is regarded as the slope in the relation  $\langle p_T \rangle = \langle p_T \rangle_0 + \beta_T \overline{m}$ , where  $\langle p_T \rangle$  denotes the mean value of transverse momenta  $p_T$ ,  $\langle p_T \rangle_0$  denotes the mean transverse momentum in the case of zero flow velocity, and  $\overline{m}$  denotes the mean moving mass. The mean flow velocity  $\beta$  is regarded as the slope in the relation  $\langle p \rangle = \langle p \rangle_0 + \beta \overline{m}$ , where  $\langle p \rangle$  denotes the mean value of momenta  $p$  and  $\langle p \rangle_0$  denotes the mean momentum in the case of zero flow velocity. Although the mean transverse radial flow and mean transverse flow are not exactly the same, we use the same symbol to denote their velocities and neglect the difference between them. In fact, the mean transverse radial flow contains only the isotropic flow, and the mean transverse flow contains both the isotropic and anisotropic flows. The isotropic flow is mainly caused by isotropic expansion of the interacting system, and the anisotropic flow is mainly caused by anisotropic squeeze between two incoming nuclei.

We are interested in the coincidence and difference among the four methods in the extractions of  $T_0$  and  $\beta_T$ . In this paper, we shall use the four methods to extract  $T_0$  and  $\beta_T$  from the  $p_T$  spectra of identified particles produced in central and peripheral gold-gold (Au-Au) collisions at the center-of-mass energy per nucleon pair  $\sqrt{s_{NN}} = 200$  GeV (the top RHIC energy) and in central and peripheral lead-lead (Pb-Pb) collisions at  $\sqrt{s_{NN}} = 2.76$  TeV (one of the LHC energies). The model results on the  $p_T$  spectra are compared with the experimental data of the PHENIX [25], STAR [26, 27], and ALICE Collaborations [28, 29], and the model results on  $T_0$  and  $\beta_T$  in different collisions and by different methods are compared each other.

The rest part of this paper is structured as follows. The formalism and method are shortly described in

section 2. Results and discussion are given in section 3. Finally, we summarize our main observations and conclusions in section 4.

## 2 Formalism and method

The four methods can be found in related references [11–20]. To give a whole representation of this paper, we present directly and concisely the four methods in the following. In the representation, some quantities such as the kinetic freeze-out temperature, the mean transverse (radial) flow velocity, and the effective temperature in different methods are uniformly denoted by  $T_0$ ,  $\beta_T$ , and  $T$ , respectively, though different methods correspond to different values. All of the model descriptions are presented at the mid-rapidity which uses the rapidity  $y \approx 0$  and results in  $\cosh(y) \approx 1$  which appears in some methods. At the same time, the spin property and chemical potential in the  $p_T$  spectra are neglected due to their small influences in high energy collisions. This means that we can give up the Fermi-Dirac and Bose-Einstein distributions, and use only the Boltzmann distribution in the case of considering the standard distribution.

According to refs. [11–13], the BGBW model results in the  $p_T$  distribution to be

$$f_1(p_T) = C_1 p_T m_T \int_0^R r dr \times I_0 \left[ \frac{p_T \sinh(\rho)}{T_0} \right] K_1 \left[ \frac{m_T \cosh(\rho)}{T_0} \right], \quad (1)$$

where  $C_1$  is the normalized constant which results in  $\int_0^\infty f_1(p_T) dp_T = 1$ ,  $I_0$  and  $K_1$  are the modified Bessel functions of the first and second kinds respectively,  $m_T = \sqrt{p_T^2 + m_0^2}$  is the transverse mass,  $\rho = \tanh^{-1}[\beta(r)]$  is the boost angle,  $\beta(r) = \beta_S (r/R)^{n_0}$  is a self-similar flow profile,  $\beta_S$  is the flow velocity on the surface of the thermal source,  $r/R$  is the relative radial position in the thermal source, and  $n_0$  is a free parameter which is customarily chosen to be 2 [11] due to the quadratic profile resembling the solutions of hydrodynamics closest [30]. Generally,  $\beta_T = (2/R^2) \int_0^R r \beta(r) dr = 2\beta_S / (n_0 + 2)$ . In the case of  $n_0 = 2$  as used in ref. [11], we have  $\beta_T = 0.5\beta_S$  [31].

According to refs. [14], the TBW model results in

the  $p_T$  distribution to be

$$f_2(p_T) = C_2 p_T m_T \int_{-\pi}^{\pi} d\phi \int_0^R r dr \left\{ 1 + \frac{q-1}{T_0} [m_T \cosh(\rho) - p_T \sinh(\rho) \cos(\phi)] \right\}^{-q/(q-1)}, \quad (2)$$

where  $C_2$  is the normalized constant which results in  $\int_0^\infty f_2(p_T) dp_T = 1$ ,  $q$  is an entropy index characterizing the degree of non-equilibrium, and  $\phi$  denotes the azimuth. In the case of  $n_0 = 1$  as used in ref. [14], we have  $\beta_T = 2\beta_S/(n_0 + 2) = (2/3)\beta_S$  due to the same flow profile as in the BGBW model. We would like to point out that the index  $-q/(q-1)$  in Eq. (2) replaced  $-1/(q-1)$  in ref. [14] due to  $q$  being very close to 1. In fact, the difference between the results corresponding to  $-q/(q-1)$  and  $-1/(q-1)$  are small in the Tsallis distribution [32].

According to refs. [15, 16], the improved Tsallis distribution in terms of  $p_T$  is

$$f_3(p_T) = C_3 \left\{ 2T_0[rI_0(s)K_1(r) - sI_1(s)K_0(r)] - (q-1)T_0r^2I_0(s)[K_0(r) + K_2(r)] + 4(q-1)T_0rsI_1(s)K_1(r) - (q-1)T_0s^2K_0(r)[I_0(s) + I_2(s)] + \frac{(q-1)}{4}T_0r^3I_0(s)[K_3(r) + 3K_1(r)] - \frac{3(q-1)}{2}T_0r^2s[K_2(r) + K_0(r)]I_1(s) + \frac{3(q-1)}{2}T_0s^2r[I_0(s) + I_2(s)]K_1(r) - \frac{(q-1)}{4}T_0s^3[I_3(s) + 3I_1(s)]K_0(r) \right\}, \quad (3)$$

where  $C_3$  is the normalized constant which results in  $\int_0^\infty f_3(p_T) dp_T = 1$ ,  $r \equiv \gamma m_T/T_0$ ,  $s \equiv \gamma \beta_T p_T/T_0$ ,  $\gamma = 1/\sqrt{1-\beta_T^2}$ , and  $I_{0-3}(s)$  and  $K_{0-3}(r)$  are the modified Bessel functions of the first and second kinds respectively.

As for the alternative method [12, 17–20, 22–24], to use the relations  $T = T_0 + am_0$ ,  $\langle p_T \rangle = \langle p_T \rangle_0 + \beta_T \bar{m}$ , and  $\langle p \rangle = \langle p \rangle_0 + \beta \bar{m}$ , we can choose the standard and Tsallis distributions to fit the  $p_T$  spectra of identified particles produced in high energy collisions. Because we give up the Fermi-Dirac and Bose-Einstein distributions, only the Boltzmann distribution is used in the case of considering the standard distribution in the present work. Both the Boltzmann and Tsallis distributions have more

than one forms. We choose the form of Boltzmann distribution [33]

$$f_{4a}(p_T) = C_{4a} p_T m_T \exp\left(-\frac{m_T}{T}\right) \quad (4)$$

and the form of Tsallis distribution [32, 33]

$$f_{4b}(p_T) = C_{4b} p_T m_T \left(1 + \frac{q-1}{T} m_T\right)^{-q/(q-1)}, \quad (5)$$

where  $C_{4a}$  and  $C_{4b}$  are the normalized constants which result in  $\int_0^\infty f_{4a}(p_T) dp_T = 1$  and  $\int_0^\infty f_{4b}(p_T) dp_T = 1$  respectively.

It should be noticed that the above five distributions are only valid for the spectra in a low- $p_T$  range. That is, they describe only the soft excitation process. Even if for the soft process, the Boltzmann distribution is not always enough to fit the  $p_T$  spectra in some cases. In fact, two- or three-component Boltzmann distribution can be used if necessary, in which  $T$  is the average weighted the effective temperatures obtained from different components. We have

$$f_{4a}(p_T) = \sum_{i=1}^l k_i C_{4ai} p_T m_T \exp\left(-\frac{m_T}{T_i}\right) \quad (6)$$

and

$$T = \sum_{i=1}^l k_i T_i, \quad (7)$$

where  $l = 2$  or  $3$  denotes the number of components, and  $k_i$ ,  $C_{4ai}$ , and  $T_i$  denote the contribution ratio (relative contribution or fraction), normalization constant, and effective temperature related to the  $i$ -th component, respectively. As can be seen in the next section, Eqs. (6) and (7) are not needed in the present work due to only simple component Boltzmann distribution, i.e. Eq. (4), is used in the analyses. We present here Eqs. (6) and (7) to point out a possible application in future.

For the spectra in a wide  $p_T$  range which contains low and high  $p_T$  regions, we have to consider the contribution of hard scattering process. Generally, the contribution of hard process is parameterized to an inverse power-law

$$f_H(p_T) = A p_T \left(1 + \frac{p_T}{p_0}\right)^{-n} \quad (8)$$

which is resulted from the QCD (quantum chromodynamics) calculation [34–36], where  $p_0$  and  $n$  are free parameters, and  $A$  is the normalized constant which depends on  $p_0$  and  $n$  and results in  $\int_0^\infty f_H(p_T) dp_T = 1$ .

To describe the spectra in a wide  $p_T$  range, we can use a superposition of both contributions of soft and

hard processes. The contribution of soft process is described by one of the BGBW model, the TBW model, the improved Tsallis distribution, the Boltzmann distribution or two- or three-component Boltzmann distribution, and the Tsallis distribution, while the contribution of hard process is described by the inverse power-law. We have the superposition

$$f_0(p_T) = kf_S(p_T) + (1 - k)f_H(p_T), \quad (9)$$

where  $k$  denotes the contribution ratio of the soft process and results naturally in  $\int_0^\infty f_0(p_T)dp_T = 1$ , and  $f_S(p_T)$  denotes one of the five distributions discussed in the four methods.

It should be noted that Eq. (9) and its components  $f_S(p_T)$  and  $f_H(p_T)$  are probability density functions. The experimental quantity of  $p_T$  distribution has mainly three forms,  $dN/dp_T$ ,  $d^2N/(dydp_T)$ , and  $(2\pi p_T)^{-1}d^2N/(dydp_T)$ , where  $N$  denotes the number of particles and  $dy$  is approximately treated as a constant due to it being usually a given and small value at the mid-rapidity. To connect Eq. (9) with  $dN/dp_T$ , we need a normalization constant  $N_0$ . To connect Eq. (9) with  $d^2N/(dydp_T)$ , we need another normalization constant  $N_0$ . To connect Eq. (9) with  $(2\pi p_T)^{-1}d^2N/(dydp_T)$ , we have to rewrite Eq. (9) to  $f_0(p_T)/p_T = [kf_S(p_T) + (1 - k)f_H(p_T)]/p_T$  and compare the right side of the new equation with the data with a new normalization constant  $N_0$ .

### 3 Results and discussion

Figure 1 presents the transverse momentum spectra,  $(2\pi p_T)^{-1}d^2N/(dydp_T)$ , of (a)-(c) positively charged pions ( $\pi^+$ ), positively charged kaons ( $K^+$ ), neutral kaons ( $K_S^0$  only), and protons ( $p$ ), as well as (b)-(d) negatively charged pions ( $\pi^-$ ), negatively charged kaons ( $K^-$ ), neutral kaons ( $K_S^0$  only), and antiprotons ( $\bar{p}$ ) produced in (a)-(b) central (0–5% and 0–12%) and (c)-(d) peripheral (80–92% and 60–80%) Au-Au collisions at  $\sqrt{s_{NN}} = 200$  GeV, where the spectra for different types of particles and for the same or similar particles in different conditions are multiplied by different amounts shown in the panels for the clarity and normalization. The closed symbols represent the experimental data of the PHENIX Collaboration measured in the pseudorapidity range  $|\eta| < 0.35$  [25]. The open symbols represent the STAR data measured in the rapidity range  $|y| < 0.5$  [26, 27], where the data for  $K^+$  and  $K^-$  are

not available and the data for  $K_S^0$  in (a)-(c) and (b)-(d) are the same. The solid, dashed, dotted, dashed-dotted, and dashed-dotted-dotted curves are our results calculated by using the superpositions of i) the BGBW model (Eq. (1)) and inverse power-law (Eq. (8)), ii) the TBW model (Eq. (2)) and inverse power-law, iii) the improved Tsallis distribution (Eq. (3)) and inverse power-law, iv)<sub>a</sub> the Boltzmann distribution (Eq. (4)) and inverse power-law, as well as iv)<sub>b</sub> the Tsallis distribution (Eq. (5)) and inverse power-law, respectively. These different superpositions are also different methods for fitting the data. The values of free parameters  $T_0$ ,  $\beta_T$ ,  $k$ ,  $p_0$ , and  $n$ , normalization constant  $N_0$  which is used to fit the data by a more accurate method comparing with Ref. [37], and  $\chi^2$  per degree of freedom ( $\chi^2/\text{dof}$ ) corresponding to the fit of method i) are listed in Table 1; the values of  $T_0$ ,  $q$ ,  $\beta_T$ ,  $k$ ,  $p_0$ ,  $n$ ,  $N_0$ , and  $\chi^2/\text{dof}$  corresponding to the methods ii) and iii) are listed in Tables 2 and 3 respectively; the values of  $T$ ,  $k$ ,  $p_0$ ,  $n$ ,  $N_0$ , and  $\chi^2/\text{dof}$  corresponding to the methods iv)<sub>a</sub> are listed in Table 4; and the values of  $T$ ,  $q$ ,  $k$ ,  $p_0$ ,  $n$ ,  $N_0$ , and  $\chi^2/\text{dof}$  corresponding to the methods iv)<sub>b</sub> are listed in Table 5. One can see that, in most cases, all of the considered methods describe approximately the  $p_T$  spectra of identified particles produced in central and peripheral Au-Au collisions at  $\sqrt{s_{NN}} = 200$  GeV.

Figure 2 is the same as Fig. 1, but it shows the spectra,  $(1/N_{EV})(2\pi p_T)^{-1}d^2N/(dydp_T)$ , of (a)-(c)  $\pi^+$  ( $\pi^+ + \pi^-$ ),  $K^+$  ( $K^+ + K^-$ ), and  $p$  ( $p + \bar{p}$ ), as well as (b)-(d)  $\pi^-$  ( $\pi^+ + \pi^-$ ),  $K^-$  ( $K^+ + K^-$ ),  $\bar{p}$  ( $p + \bar{p}$ ) produced in (a)-(b) central (0–5%) and (c)-(d) peripheral (80–90% and 60–80%) Pb-Pb collisions at  $\sqrt{s_{NN}} = 2.76$  TeV, where  $N_{EV}$  on the vertical axis denotes the number of events, which is usually omitted. The closed (open) symbols represent the experimental data of the ALICE Collaboration measured in  $|y| < 0.5$  [28] (in  $|\eta| < 0.8$  for high  $p_T$  region and in  $|y| < 0.5$  for low  $p_T$  region [29]). The data for  $\pi^+ + \pi^-$ ,  $K^+ + K^-$ , and  $p + \bar{p}$  in (a)-(c) and (b)-(d) are the same. One can see that, in most cases, all of the considered methods describe approximately the  $p_T$  spectra of identified particles produced in central and peripheral Pb-Pb collisions at  $\sqrt{s_{NN}} = 2.76$  TeV. Because the values of  $\chi^2/\text{dof}$  in most cases are greater than 2 and sometimes as large as 20.5, the fits in Figs. 1 and 2 are only approximate and qualitative. The large values of  $\chi^2/\text{dof}$  in the present work are caused by two factors which are the very small errors in the data and large dispersion between the curve and data in some

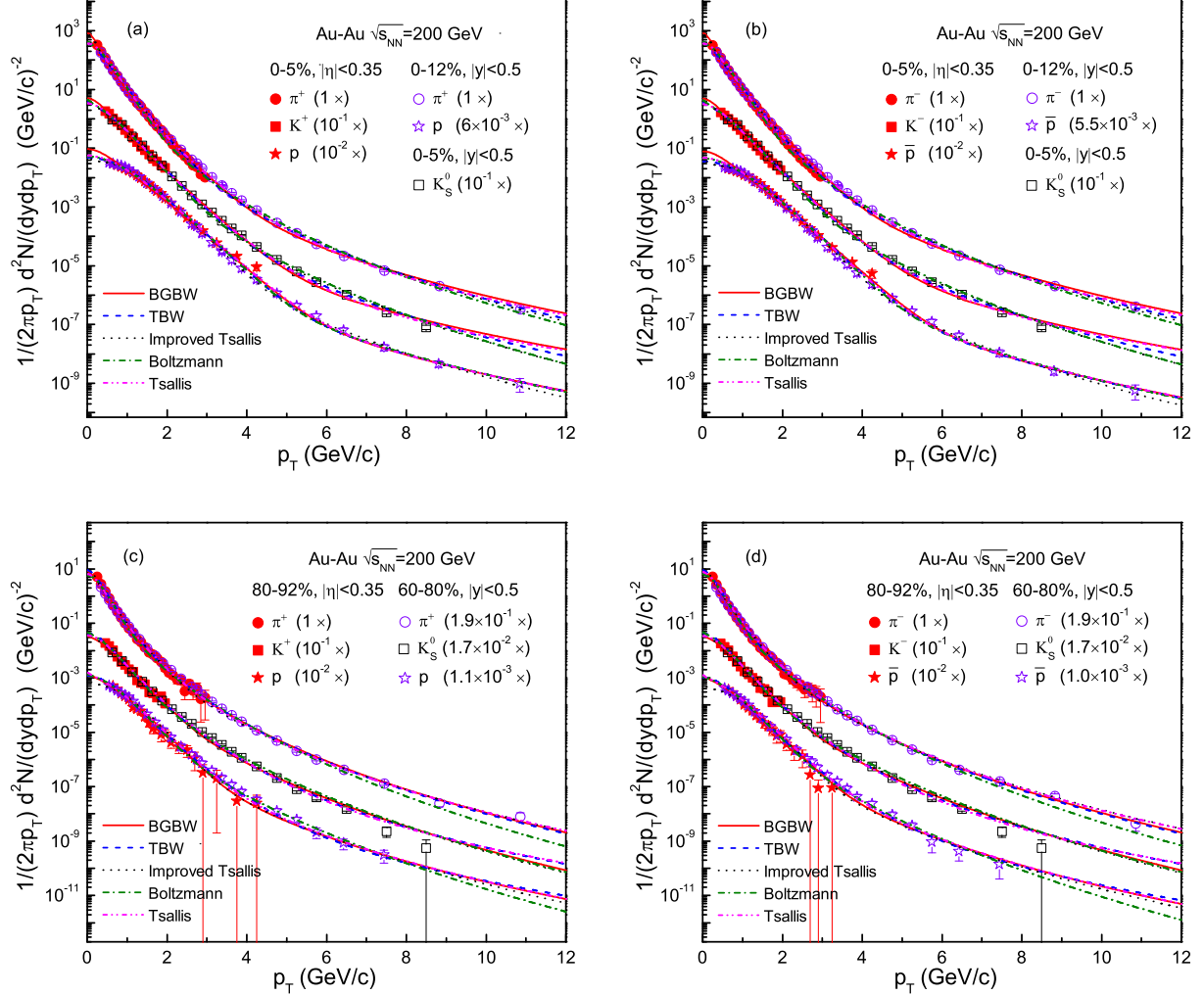


Fig. 1. (Colour figure online) Transverse momentum spectra of (a)-(c)  $\pi^+$ ,  $K^+$ ,  $K_S^0$ , and  $p$ , as well as (b)-(d)  $\pi^-$ ,  $K^-$ ,  $K_S^0$ , and  $\bar{p}$  produced in (a)-(b) central (0–5% and 0–12%) and (c)-(d) peripheral (80–92% and 60–80%) Au-Au collisions at  $\sqrt{s_{NN}} = 200$  GeV, where the spectra for different types of particles and for the same or similar particles in different conditions are multiplied by different amounts shown in the panels for the clarity and normalization. The closed symbols represent the experimental data of the PHENIX Collaboration measured in  $|\eta| < 0.35$  [25]. The open symbols represent the STAR data measured in  $|y| < 0.5$  [26, 27], where the data for  $K^+$  and  $K^-$  are not available and the data for  $K_S^0$  in (a)-(c) and (b)-(d) are the same. The solid, dashed, dotted, dashed-dotted, and dashed-dotted-dotted curves are our results calculated by using the methods i), ii), iii), iv)<sub>a</sub>, and iv)<sub>b</sub>, respectively.

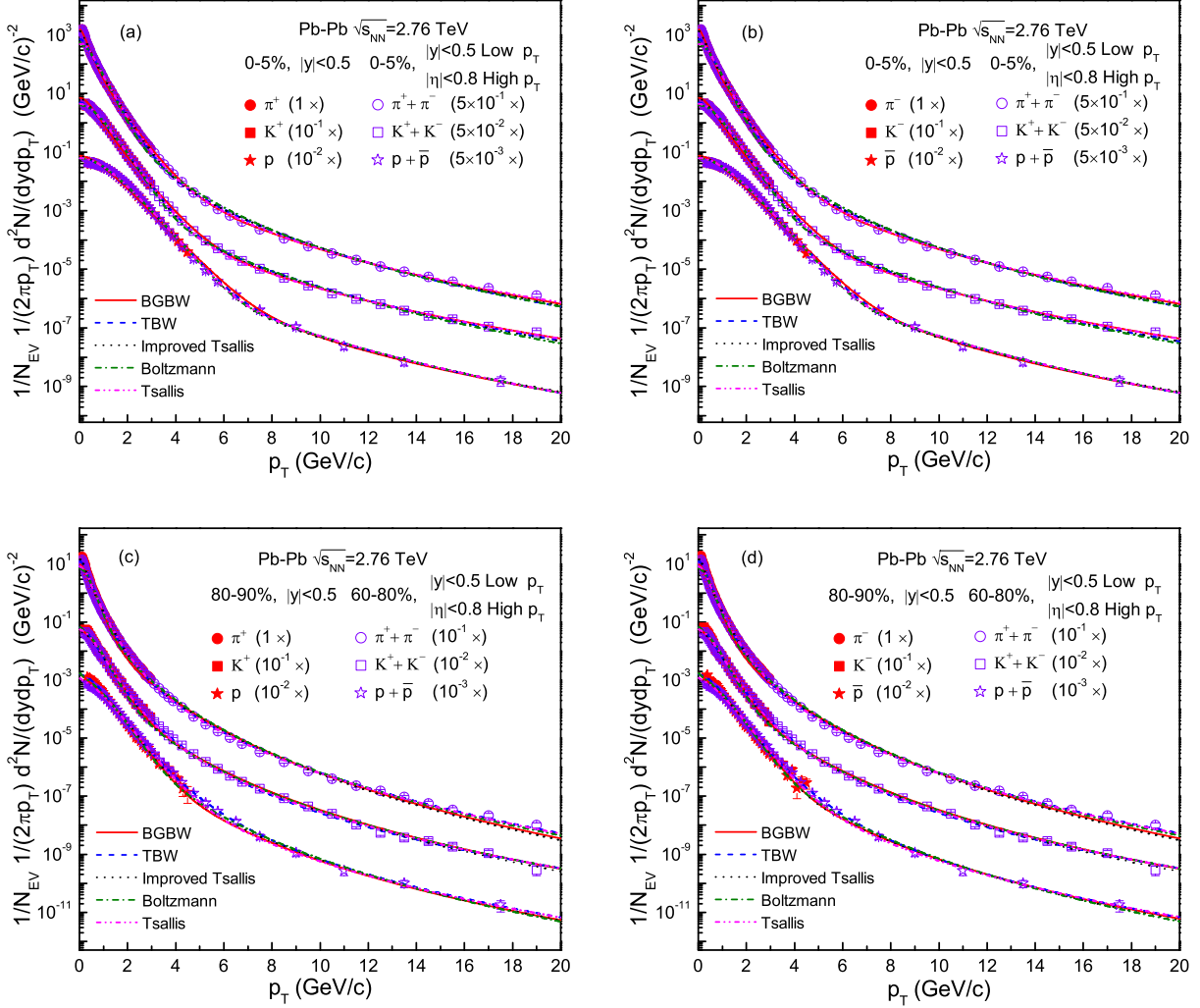


Fig. 2. (Colour figure online) Same as Fig. 1, but showing the spectra of (a)-(c)  $\pi^+$  ( $\pi^+ + \pi^-$ ),  $K^+$  ( $K^+ + K^-$ ), and  $p$  ( $p + \bar{p}$ ), as well as (b)-(d)  $\pi^-$  ( $\pi^+ + \pi^-$ ),  $K^-$  ( $K^+ + K^-$ ),  $\bar{p}$  ( $p + \bar{p}$ ) produced in (a)-(b) central (0–5%) and (c)-(d) peripheral (80–90% and 60–80%) Pb-Pb collisions at  $\sqrt{s_{NN}} = 2.76$  TeV, where  $N_{EV}$  on the vertical axis denotes the number of events, which is usually omitted. The closed (open) symbols represent the experimental data of the ALICE Collaboration measured in  $|y| < 0.5$  [28] (in  $|\eta| < 0.8$  for high  $p_T$  region and in  $|y| < 0.5$  for low  $p_T$  region [29]). The data for  $\pi^+ + \pi^-$ ,  $K^+ + K^-$ , and  $p + \bar{p}$  in (a)-(c) and (b)-(d) are the same.

Table 1. Values of free parameters ( $T_0$ ,  $\beta_T$ ,  $k$ ,  $p_0$ , and  $n$ ), normalization constant ( $N_0$ ), and  $\chi^2/\text{dof}$  corresponding to the fits of method i) in Figs. 1 and 2, where  $n_0 = 2$  in the self-similar flow profile is used as ref. [11].

Fig.	Cent.	Main Part.	$T_0$ (GeV)	$\beta_T$ (c)	$k$	$p_0$ (GeV/c)	$n$	$N_0$	$\chi^2/\text{dof}$
1(a)	Central	$\pi^+$	$0.113 \pm 0.004$	$0.413 \pm 0.006$	$0.988 \pm 0.003$	$2.075 \pm 0.062$	$9.015 \pm 0.148$	$985.309 \pm 75.105$	2.708
		$K^+$	$0.124 \pm 0.005$	$0.408 \pm 0.006$	$0.975 \pm 0.004$	$1.295 \pm 0.058$	$7.375 \pm 0.128$	$65.180 \pm 3.873$	7.300
		$p$	$0.127 \pm 0.005$	$0.392 \pm 0.006$	$0.989 \pm 0.003$	$2.485 \pm 0.076$	$8.775 \pm 0.136$	$12.611 \pm 0.636$	10.729
1(b)	Central	$\pi^-$	$0.113 \pm 0.004$	$0.413 \pm 0.006$	$0.988 \pm 0.003$	$2.075 \pm 0.062$	$9.015 \pm 0.148$	$985.309 \pm 75.105$	2.792
		$K^-$	$0.124 \pm 0.005$	$0.408 \pm 0.006$	$0.975 \pm 0.004$	$1.295 \pm 0.058$	$7.375 \pm 0.128$	$63.109 \pm 3.589$	9.267
		$\bar{p}$	$0.125 \pm 0.005$	$0.392 \pm 0.006$	$0.990 \pm 0.003$	$2.465 \pm 0.076$	$8.895 \pm 0.136$	$10.572 \pm 0.599$	20.512
1(c)	Peripheral	$\pi^+$	$0.160 \pm 0.004$	$0.000_{-0}^{+0.016}$	$0.754 \pm 0.009$	$2.012 \pm 0.069$	$10.803 \pm 0.143$	$9.794 \pm 0.726$	4.237
		$K^+$	$0.238 \pm 0.005$	$0.000_{-0}^{+0.016}$	$0.825 \pm 0.009$	$3.383 \pm 0.089$	$12.313 \pm 0.166$	$0.424 \pm 0.029$	8.755
		$p$	$0.251 \pm 0.005$	$0.000_{-0}^{+0.016}$	$0.851 \pm 0.011$	$2.006 \pm 0.065$	$9.466 \pm 0.139$	$0.167 \pm 0.012$	1.434
1(d)	Peripheral	$\pi^-$	$0.160 \pm 0.004$	$0.000_{-0}^{+0.016}$	$0.754 \pm 0.009$	$2.012 \pm 0.069$	$10.803 \pm 0.143$	$9.794 \pm 0.726$	3.792
		$K^-$	$0.238 \pm 0.005$	$0.000_{-0}^{+0.016}$	$0.825 \pm 0.009$	$3.383 \pm 0.089$	$12.313 \pm 0.166$	$0.424 \pm 0.029$	7.469
		$\bar{p}$	$0.251 \pm 0.005$	$0.000_{-0}^{+0.016}$	$0.851 \pm 0.011$	$2.106 \pm 0.066$	$9.766 \pm 0.141$	$0.134 \pm 0.007$	0.834
2(a)	Central	$\pi^+$	$0.128 \pm 0.004$	$0.434 \pm 0.007$	$0.992 \pm 0.002$	$2.775 \pm 0.091$	$7.435 \pm 0.133$	$1771.569 \pm 112.825$	1.200
		$K^+$	$0.187 \pm 0.004$	$0.390 \pm 0.006$	$0.993 \pm 0.002$	$3.575 \pm 0.098$	$7.135 \pm 0.128$	$92.874 \pm 6.429$	3.647
		$p$	$0.429 \pm 0.005$	$0.145 \pm 0.005$	$0.976 \pm 0.005$	$2.485 \pm 0.088$	$7.375 \pm 0.136$	$10.188 \pm 0.445$	7.472
2(b)	Central	$\pi^-$	$0.128 \pm 0.004$	$0.434 \pm 0.007$	$0.992 \pm 0.002$	$2.775 \pm 0.091$	$7.435 \pm 0.133$	$1771.569 \pm 112.825$	1.221
		$K^-$	$0.187 \pm 0.004$	$0.390 \pm 0.006$	$0.993 \pm 0.002$	$3.575 \pm 0.098$	$7.135 \pm 0.128$	$92.874 \pm 6.429$	3.288
		$\bar{p}$	$0.428 \pm 0.005$	$0.145 \pm 0.005$	$0.976 \pm 0.005$	$2.485 \pm 0.088$	$7.375 \pm 0.136$	$10.209 \pm 0.446$	6.875
2(c)	Peripheral	$\pi^+$	$0.183 \pm 0.004$	$0.000_{-0}^{+0.017}$	$0.909 \pm 0.009$	$2.793 \pm 0.089$	$8.985 \pm 0.133$	$12.144 \pm 0.705$	16.627
		$K^+$	$0.272 \pm 0.004$	$0.000_{-0}^{+0.017}$	$0.835 \pm 0.009$	$2.375 \pm 0.085$	$7.885 \pm 0.165$	$0.707 \pm 0.028$	2.808
		$p$	$0.338 \pm 0.004$	$0.000_{-0}^{+0.017}$	$0.836 \pm 0.009$	$1.875 \pm 0.078$	$7.705 \pm 0.138$	$0.183 \pm 0.011$	2.752
2(d)	Peripheral	$\pi^-$	$0.183 \pm 0.004$	$0.000_{-0}^{+0.017}$	$0.909 \pm 0.009$	$2.793 \pm 0.089$	$8.985 \pm 0.133$	$12.144 \pm 0.705$	16.734
		$K^-$	$0.272 \pm 0.004$	$0.000_{-0}^{+0.017}$	$0.835 \pm 0.009$	$2.375 \pm 0.085$	$7.885 \pm 0.165$	$0.707 \pm 0.028$	3.041
		$\bar{p}$	$0.342 \pm 0.004$	$0.000_{-0}^{+0.017}$	$0.815 \pm 0.009$	$1.875 \pm 0.078$	$7.705 \pm 0.138$	$0.185 \pm 0.012$	2.602

Table 2. Values of free parameters ( $T_0$ ,  $q$ ,  $\beta_T$ ,  $k$ ,  $p_0$ , and  $n$ ), normalization constant ( $N_0$ ), and  $\chi^2/\text{dof}$  corresponding to the fits of method ii) in Figs. 1 and 2, where  $n_0 = 1$  is used as ref. [14].

Fig.	Cent.	Main Part.	$T_0$ (GeV)	$q$	$\beta_T$ (c)	$k$	$p_0$ (GeV/c)	$n$	$N_0$	$\chi^2/\text{dof}$
1(a)	Central	$\pi^+$	$0.108 \pm 0.004$	$1.008 \pm 0.005$	$0.472 \pm 0.010$	$0.882 \pm 0.008$	$1.775 \pm 0.069$	$9.895 \pm 0.143$	$486.350 \pm 40.221$	4.082
		$K^+$	$0.113 \pm 0.004$	$1.020 \pm 0.005$	$0.469 \pm 0.010$	$0.901 \pm 0.006$	$1.875 \pm 0.072$	$9.405 \pm 0.139$	$44.575 \pm 2.808$	6.564
		$p$	$0.119 \pm 0.004$	$1.011 \pm 0.004$	$0.469 \pm 0.008$	$0.989 \pm 0.003$	$2.885 \pm 0.082$	$9.275 \pm 0.136$	$7.214 \pm 0.368$	1.665
1(b)	Central	$\pi^-$	$0.108 \pm 0.004$	$1.008 \pm 0.005$	$0.472 \pm 0.010$	$0.882 \pm 0.008$	$1.775 \pm 0.069$	$9.895 \pm 0.143$	$486.350 \pm 40.221$	3.856
		$K^-$	$0.113 \pm 0.004$	$1.020 \pm 0.005$	$0.469 \pm 0.010$	$0.901 \pm 0.006$	$1.875 \pm 0.072$	$9.405 \pm 0.139$	$42.837 \pm 2.808$	5.939
		$\bar{p}$	$0.121 \pm 0.004$	$1.010 \pm 0.004$	$0.469 \pm 0.008$	$0.991 \pm 0.003$	$2.885 \pm 0.082$	$9.305 \pm 0.134$	$5.369 \pm 0.354$	6.643
1(c)	Peripheral	$\pi^+$	$0.099 \pm 0.004$	$1.078 \pm 0.005$	$0.000_{-0}^{+0.036}$	$0.862 \pm 0.008$	$2.198 \pm 0.089$	$10.982 \pm 0.161$	$11.341 \pm 0.747$	3.221
		$K^+$	$0.119 \pm 0.004$	$1.088 \pm 0.004$	$0.000_{-0}^{+0.036}$	$0.985 \pm 0.008$	$1.983 \pm 0.078$	$8.253 \pm 0.138$	$0.589 \pm 0.053$	4.002
		$p$	$0.132 \pm 0.004$	$1.064 \pm 0.005$	$0.000_{-0}^{+0.036}$	$0.985 \pm 0.004$	$2.010 \pm 0.088$	$7.966 \pm 0.129$	$0.171 \pm 0.014$	0.940
1(d)	Peripheral	$\pi^-$	$0.099 \pm 0.004$	$1.078 \pm 0.005$	$0.000_{-0}^{+0.036}$	$0.862 \pm 0.008$	$2.198 \pm 0.089$	$10.982 \pm 0.161$	$11.341 \pm 0.747$	2.924
		$K^-$	$0.119 \pm 0.004$	$1.088 \pm 0.004$	$0.000_{-0}^{+0.036}$	$0.985 \pm 0.008$	$1.983 \pm 0.078$	$8.253 \pm 0.138$	$0.589 \pm 0.053$	3.652
		$\bar{p}$	$0.124 \pm 0.004$	$1.067 \pm 0.005$	$0.000_{-0}^{+0.036}$	$0.983 \pm 0.004$	$2.018 \pm 0.088$	$8.166 \pm 0.129$	$0.144 \pm 0.014$	0.552
2(a)	Central	$\pi^+$	$0.109 \pm 0.004$	$1.009 \pm 0.005$	$0.525 \pm 0.009$	$0.977 \pm 0.005$	$2.585 \pm 0.086$	$7.875 \pm 0.122$	$917.576 \pm 91.809$	6.313
		$K^+$	$0.145 \pm 0.005$	$1.004 \pm 0.003$	$0.500 \pm 0.009$	$0.984 \pm 0.004$	$3.255 \pm 0.091$	$7.508 \pm 0.119$	$66.904 \pm 6.743$	0.580
		$p$	$0.178 \pm 0.005$	$1.002 \pm 0.001$	$0.500 \pm 0.008$	$0.993 \pm 0.002$	$4.975 \pm 0.099$	$8.725 \pm 0.121$	$8.981 \pm 0.254$	3.509
2(b)	Central	$\pi^-$	$0.109 \pm 0.004$	$1.009 \pm 0.005$	$0.525 \pm 0.009$	$0.977 \pm 0.005$	$2.585 \pm 0.086$	$7.875 \pm 0.122$	$917.576 \pm 91.809$	6.249
		$K^-$	$0.145 \pm 0.005$	$1.004 \pm 0.003$	$0.500 \pm 0.009$	$0.985 \pm 0.004$	$3.255 \pm 0.091$	$7.508 \pm 0.119$	$66.904 \pm 6.743$	0.570
		$\bar{p}$	$0.178 \pm 0.005$	$1.002 \pm 0.001$	$0.500 \pm 0.008$	$0.993 \pm 0.002$	$4.975 \pm 0.099$	$8.725 \pm 0.121$	$8.981 \pm 0.254$	3.253
2(c)	Peripheral	$\pi^+$	$0.102 \pm 0.004$	$1.108 \pm 0.005$	$0.000_{-0}^{+0.018}$	$0.976 \pm 0.005$	$3.003 \pm 0.089$	$8.335 \pm 0.118$	$15.628 \pm 0.563$	10.532
		$K^+$	$0.141 \pm 0.005$	$1.099 \pm 0.005$	$0.000_{-0}^{+0.018}$	$0.906 \pm 0.005$	$1.875 \pm 0.071$	$7.038 \pm 0.109$	$0.820 \pm 0.063$	1.149
		$p$	$0.172 \pm 0.005$	$1.076 \pm 0.005$	$0.000_{-0}^{+0.018}$	$0.958 \pm 0.005$	$2.375 \pm 0.088$	$7.575 \pm 0.119$	$0.212 \pm 0.017$	4.623
2(d)	Peripheral	$\pi^-$	$0.102 \pm 0.004$	$1.108 \pm 0.005$	$0.000_{-0}^{+0.018}$	$0.976 \pm 0.005$	$3.003 \pm 0.089$	$8.335 \pm 0.118$	$15.628 \pm 0.563$	10.481
		$K^-$	$0.141 \pm 0.005$	$1.099 \pm 0.005$	$0.000_{-0}^{+0.018}$	$0.906 \pm 0.005$	$1.875 \pm 0.071$	$7.038 \pm 0.109$	$0.820 \pm 0.063$	1.279
		$\bar{p}$	$0.172 \pm 0.005$	$1.076 \pm 0.005$	$0.000_{-0}^{+0.018}$	$0.958 \pm 0.005$	$2.375 \pm 0.088$	$7.575 \pm 0.119$	$0.212 \pm 0.017$	4.832

Table 3. Values of free parameters ( $T_0$ ,  $q$ ,  $\beta_T$ ,  $k$ ,  $p_0$ , and  $n$ ), normalization constant ( $N_0$ ), and  $\chi^2/\text{dof}$  corresponding to the fits of method iii) in Figs. 1 and 2.

Fig.	Cent.	Main Part.	$T_0$ (GeV)	$q$	$\beta_T$ (c)	$k$	$p_0$ (GeV/c)	$n$	$N_0$	$\chi^2/\text{dof}$
1(a)	Central	$\pi^+$	$0.113 \pm 0.006$	$1.017 \pm 0.007$	$0.634 \pm 0.009$	$0.939 \pm 0.008$	$2.475 \pm 0.088$	$11.091 \pm 0.165$	$746.564 \pm 89.743$	2.986
		$K^+$	$0.116 \pm 0.006$	$1.040 \pm 0.007$	$0.634 \pm 0.009$	$0.902 \pm 0.008$	$3.675 \pm 0.091$	$12.995 \pm 0.172$	$32.457 \pm 5.734$	9.781
		$p$	$0.121 \pm 0.006$	$1.024 \pm 0.007$	$0.634 \pm 0.009$	$0.916 \pm 0.008$	$2.985 \pm 0.090$	$11.225 \pm 0.162$	$5.365 \pm 0.677$	1.249
1(b)	Central	$\pi^-$	$0.113 \pm 0.006$	$1.017 \pm 0.007$	$0.634 \pm 0.009$	$0.939 \pm 0.008$	$2.475 \pm 0.088$	$11.091 \pm 0.165$	$746.564 \pm 89.743$	2.700
		$K^-$	$0.116 \pm 0.006$	$1.040 \pm 0.007$	$0.634 \pm 0.009$	$0.900 \pm 0.008$	$3.675 \pm 0.091$	$12.995 \pm 0.172$	$31.193 \pm 5.698$	8.100
		$\bar{p}$	$0.121 \pm 0.006$	$1.024 \pm 0.007$	$0.634 \pm 0.009$	$0.909 \pm 0.008$	$2.985 \pm 0.090$	$11.525 \pm 0.162$	$8.294 \pm 1.243$	2.878
1(c)	Peripheral	$\pi^+$	$0.102 \pm 0.006$	$1.031 \pm 0.007$	$0.583 \pm 0.009$	$0.891 \pm 0.008$	$2.185 \pm 0.086$	$10.632 \pm 0.148$	$10.292 \pm 1.860$	3.931
		$K^+$	$0.109 \pm 0.006$	$1.045 \pm 0.008$	$0.578 \pm 0.009$	$0.872 \pm 0.008$	$4.483 \pm 0.099$	$14.061 \pm 0.165$	$0.327 \pm 0.057$	8.529
		$p$	$0.110 \pm 0.006$	$1.053 \pm 0.008$	$0.548 \pm 0.008$	$0.901 \pm 0.008$	$3.066 \pm 0.095$	$11.166 \pm 0.126$	$0.083 \pm 0.005$	2.700
1(d)	Peripheral	$\pi^-$	$0.102 \pm 0.006$	$1.031 \pm 0.007$	$0.583 \pm 0.009$	$0.891 \pm 0.008$	$2.185 \pm 0.086$	$10.532 \pm 0.148$	$10.771 \pm 1.863$	3.751
		$K^-$	$0.109 \pm 0.006$	$1.045 \pm 0.008$	$0.578 \pm 0.009$	$0.872 \pm 0.008$	$4.483 \pm 0.099$	$14.061 \pm 0.165$	$0.327 \pm 0.057$	7.157
		$\bar{p}$	$0.110 \pm 0.006$	$1.053 \pm 0.008$	$0.548 \pm 0.008$	$0.901 \pm 0.008$	$3.066 \pm 0.095$	$11.166 \pm 0.126$	$0.055 \pm 0.005$	1.316
2(a)	Central	$\pi^+$	$0.152 \pm 0.004$	$1.011 \pm 0.004$	$0.609 \pm 0.010$	$0.981 \pm 0.007$	$2.575 \pm 0.094$	$7.775 \pm 0.145$	$1475.441 \pm 93.801$	2.682
		$K^+$	$0.158 \pm 0.004$	$1.059 \pm 0.008$	$0.609 \pm 0.010$	$0.987 \pm 0.006$	$3.575 \pm 0.102$	$7.655 \pm 0.144$	$58.904 \pm 5.207$	1.235
		$p$	$0.194 \pm 0.005$	$1.069 \pm 0.011$	$0.609 \pm 0.010$	$0.987 \pm 0.006$	$2.885 \pm 0.101$	$7.375 \pm 0.148$	$7.792 \pm 0.559$	4.833
2(b)	Central	$\pi^-$	$0.152 \pm 0.004$	$1.011 \pm 0.004$	$0.609 \pm 0.010$	$0.981 \pm 0.007$	$2.575 \pm 0.094$	$7.775 \pm 0.145$	$1475.441 \pm 93.801$	2.586
		$K^-$	$0.158 \pm 0.004$	$1.059 \pm 0.008$	$0.609 \pm 0.010$	$0.987 \pm 0.006$	$3.575 \pm 0.102$	$7.655 \pm 0.144$	$58.904 \pm 5.207$	1.083
		$\bar{p}$	$0.194 \pm 0.005$	$1.069 \pm 0.011$	$0.609 \pm 0.010$	$0.987 \pm 0.006$	$2.885 \pm 0.101$	$7.375 \pm 0.148$	$7.792 \pm 0.559$	4.482
2(c)	Peripheral	$\pi^+$	$0.118 \pm 0.005$	$1.008 \pm 0.005$	$0.630 \pm 0.009$	$0.920 \pm 0.007$	$2.903 \pm 0.103$	$9.135 \pm 0.165$	$15.956 \pm 0.981$	5.202
		$K^+$	$0.143 \pm 0.004$	$1.011 \pm 0.005$	$0.602 \pm 0.009$	$0.901 \pm 0.007$	$3.003 \pm 0.111$	$8.335 \pm 0.155$	$0.530 \pm 0.038$	1.880
		$p$	$0.163 \pm 0.005$	$1.021 \pm 0.005$	$0.559 \pm 0.009$	$0.889 \pm 0.007$	$2.375 \pm 0.099$	$8.059 \pm 0.142$	$0.102 \pm 0.006$	2.804
2(d)	Peripheral	$\pi^-$	$0.118 \pm 0.005$	$1.008 \pm 0.005$	$0.630 \pm 0.009$	$0.920 \pm 0.007$	$2.903 \pm 0.103$	$9.135 \pm 0.165$	$15.956 \pm 0.981$	5.257
		$K^-$	$0.143 \pm 0.004$	$1.011 \pm 0.005$	$0.602 \pm 0.009$	$0.901 \pm 0.007$	$3.003 \pm 0.111$	$8.335 \pm 0.155$	$0.525 \pm 0.034$	1.979
		$\bar{p}$	$0.163 \pm 0.005$	$1.021 \pm 0.005$	$0.559 \pm 0.009$	$0.889 \pm 0.007$	$2.375 \pm 0.099$	$8.059 \pm 0.142$	$0.101 \pm 0.006$	2.942

Table 4. Values of free parameters ( $T$ ,  $k$ ,  $p_0$ , and  $n$ ), normalization constant ( $N_0$ ), and  $\chi^2/\text{dof}$  corresponding to the fits of method iv)<sub>a</sub> in Figs. 1 and 2.

Fig.	Cent.	Main Part.	$T$ (GeV)	$k$	$p_0$ (GeV/c)	$n$	$N_0$	$\chi^2/\text{dof}$
1(a)	Central	$\pi^+$	$0.167 \pm 0.004$	$0.765 \pm 0.008$	$2.095 \pm 0.068$	$11.295 \pm 0.133$	$519.268 \pm 39.582$	9.637
		$K^+$	$0.235 \pm 0.004$	$0.752 \pm 0.008$	$2.915 \pm 0.068$	$12.335 \pm 0.185$	$49.650 \pm 2.890$	12.847
1(b)	Central	$p$	$0.302 \pm 0.005$	$0.983 \pm 0.005$	$2.785 \pm 0.066$	$9.475 \pm 0.176$	$7.744 \pm 0.267$	2.217
		$\pi^-$	$0.167 \pm 0.004$	$0.765 \pm 0.008$	$2.095 \pm 0.068$	$11.295 \pm 0.133$	$519.297 \pm 39.582$	9.068
		$K^-$	$0.235 \pm 0.004$	$0.750 \pm 0.008$	$2.915 \pm 0.068$	$12.335 \pm 0.185$	$47.297 \pm 2.893$	13.624
1(c)	Peripheral	$\bar{p}$	$0.296 \pm 0.005$	$0.981 \pm 0.005$	$2.715 \pm 0.066$	$9.675 \pm 0.176$	$6.516 \pm 0.272$	6.399
		$\pi^+$	$0.131 \pm 0.004$	$0.799 \pm 0.008$	$3.238 \pm 0.089$	$13.892 \pm 0.132$	$8.602 \pm 0.676$	4.243
		$K^+$	$0.185 \pm 0.004$	$0.702 \pm 0.008$	$3.483 \pm 0.086$	$13.083 \pm 0.146$	$0.556 \pm 0.035$	6.799
1(d)	Peripheral	$p$	$0.209 \pm 0.005$	$0.822 \pm 0.008$	$4.606 \pm 0.106$	$14.866 \pm 0.155$	$0.173 \pm 0.012$	0.955
		$\pi^-$	$0.131 \pm 0.004$	$0.799 \pm 0.008$	$3.238 \pm 0.089$	$13.892 \pm 0.132$	$8.602 \pm 0.676$	4.115
		$K^-$	$0.185 \pm 0.004$	$0.702 \pm 0.008$	$3.483 \pm 0.086$	$13.083 \pm 0.146$	$0.559 \pm 0.035$	6.284
2(a)	Central	$\bar{p}$	$0.209 \pm 0.005$	$0.822 \pm 0.008$	$4.606 \pm 0.106$	$15.279 \pm 0.165$	$0.139 \pm 0.012$	0.627
		$\pi^+$	$0.215 \pm 0.004$	$0.828 \pm 0.008$	$1.375 \pm 0.068$	$7.315 \pm 0.128$	$679.491 \pm 44.189$	16.706
		$K^+$	$0.299 \pm 0.005$	$0.972 \pm 0.008$	$2.945 \pm 0.090$	$7.685 \pm 0.132$	$57.722 \pm 5.536$	1.889
2(b)	Central	$p$	$0.413 \pm 0.005$	$0.993 \pm 0.002$	$4.975 \pm 0.112$	$8.725 \pm 0.146$	$8.864 \pm 0.467$	2.600
		$\pi^-$	$0.215 \pm 0.004$	$0.828 \pm 0.008$	$1.375 \pm 0.068$	$7.315 \pm 0.128$	$679.491 \pm 44.189$	16.821
		$K^-$	$0.299 \pm 0.005$	$0.972 \pm 0.008$	$2.945 \pm 0.090$	$7.685 \pm 0.132$	$57.722 \pm 5.536$	2.052
2(c)	Peripheral	$\bar{p}$	$0.413 \pm 0.005$	$0.993 \pm 0.002$	$4.975 \pm 0.112$	$8.725 \pm 0.146$	$8.864 \pm 0.467$	2.433
		$\pi^+$	$0.152 \pm 0.004$	$0.802 \pm 0.008$	$2.012 \pm 0.065$	$8.279 \pm 0.116$	$9.713 \pm 0.616$	15.656
		$K^+$	$0.219 \pm 0.004$	$0.803 \pm 0.009$	$2.035 \pm 0.092$	$7.595 \pm 0.134$	$0.822 \pm 0.052$	5.123
2(d)	Peripheral	$p$	$0.291 \pm 0.005$	$0.805 \pm 0.008$	$2.285 \pm 0.096$	$8.365 \pm 0.142$	$0.190 \pm 0.017$	3.545
		$\pi^-$	$0.152 \pm 0.004$	$0.802 \pm 0.008$	$2.012 \pm 0.065$	$8.279 \pm 0.116$	$9.713 \pm 0.616$	15.657
		$K^-$	$0.219 \pm 0.004$	$0.803 \pm 0.009$	$2.035 \pm 0.092$	$7.595 \pm 0.134$	$0.822 \pm 0.052$	5.238
		$\bar{p}$	$0.296 \pm 0.005$	$0.805 \pm 0.008$	$2.285 \pm 0.096$	$8.365 \pm 0.142$	$0.188 \pm 0.017$	3.391



Table 5. Values of free parameters ( $T$ ,  $q$ ,  $k$ ,  $p_0$ , and  $n$ ), normalization constant ( $N_0$ ), and  $\chi^2/\text{dof}$  corresponding to the fits of method iv)<sub>b</sub> in Figs. 1 and 2.

Fig.	Cent.	Main Part.	$T$ (GeV)	$q$	$k$	$p_0$ (GeV/ $c$ )	$n$	$N_0$	$\chi^2/\text{dof}$
1(a)	Central	$\pi^+$	$0.130 \pm 0.004$	$1.073 \pm 0.003$	$0.994 \pm 0.003$	$1.775 \pm 0.069$	$8.115 \pm 0.148$	$508.830 \pm 43.650$	1.731
		$K^+$	$0.184 \pm 0.005$	$1.050 \pm 0.004$	$0.984 \pm 0.005$	$1.075 \pm 0.058$	$6.775 \pm 0.135$	$45.687 \pm 2.962$	4.354
		$p$	$0.274 \pm 0.004$	$1.015 \pm 0.003$	$0.988 \pm 0.003$	$2.485 \pm 0.088$	$8.775 \pm 0.152$	$8.211 \pm 0.194$	3.268
1(b)	Central	$\pi^-$	$0.130 \pm 0.004$	$1.073 \pm 0.003$	$0.994 \pm 0.003$	$1.775 \pm 0.069$	$8.115 \pm 0.148$	$508.830 \pm 43.650$	1.648
		$K^-$	$0.184 \pm 0.005$	$1.050 \pm 0.004$	$0.982 \pm 0.005$	$1.075 \pm 0.058$	$6.775 \pm 0.135$	$42.366 \pm 2.868$	2.951
		$\bar{p}$	$0.272 \pm 0.004$	$1.012 \pm 0.003$	$0.992 \pm 0.003$	$2.985 \pm 0.090$	$9.375 \pm 0.159$	$6.764 \pm 0.189$	7.806
1(c)	Peripheral	$\pi^+$	$0.105 \pm 0.004$	$1.085 \pm 0.005$	$0.918 \pm 0.005$	$1.985 \pm 0.075$	$10.032 \pm 0.155$	$8.344 \pm 0.606$	1.855
		$K^+$	$0.137 \pm 0.004$	$1.079 \pm 0.004$	$0.990 \pm 0.006$	$1.983 \pm 0.075$	$7.853 \pm 0.136$	$0.488 \pm 0.033$	3.574
		$p$	$0.192 \pm 0.005$	$1.028 \pm 0.006$	$0.853 \pm 0.008$	$2.006 \pm 0.056$	$9.466 \pm 0.155$	$0.175 \pm 0.012$	1.165
1(d)	Peripheral	$\pi^-$	$0.105 \pm 0.004$	$1.085 \pm 0.005$	$0.918 \pm 0.005$	$1.985 \pm 0.075$	$10.032 \pm 0.155$	$8.344 \pm 0.606$	1.635
		$K^-$	$0.137 \pm 0.004$	$1.079 \pm 0.004$	$0.990 \pm 0.006$	$1.983 \pm 0.075$	$7.853 \pm 0.136$	$0.466 \pm 0.030$	2.604
		$\bar{p}$	$0.192 \pm 0.005$	$1.028 \pm 0.006$	$0.853 \pm 0.008$	$2.106 \pm 0.059$	$9.766 \pm 0.158$	$0.140 \pm 0.012$	0.715
2(a)	Central	$\pi^+$	$0.170 \pm 0.005$	$1.066 \pm 0.005$	$0.992 \pm 0.007$	$2.775 \pm 0.062$	$7.275 \pm 0.185$	$711.631 \pm 55.063$	6.847
		$K^+$	$0.264 \pm 0.006$	$1.030 \pm 0.005$	$0.993 \pm 0.002$	$3.575 \pm 0.108$	$7.135 \pm 0.203$	$62.036 \pm 5.422$	0.548
		$p$	$0.409 \pm 0.006$	$1.002 \pm 0.001$	$0.993 \pm 0.002$	$4.975 \pm 0.112$	$8.725 \pm 0.206$	$8.968 \pm 0.417$	2.813
2(b)	Central	$\pi^-$	$0.170 \pm 0.005$	$1.066 \pm 0.005$	$0.992 \pm 0.007$	$2.775 \pm 0.062$	$7.275 \pm 0.185$	$711.631 \pm 55.063$	6.813
		$K^-$	$0.264 \pm 0.006$	$1.030 \pm 0.005$	$0.993 \pm 0.002$	$3.575 \pm 0.108$	$7.135 \pm 0.203$	$62.036 \pm 5.422$	0.654
		$\bar{p}$	$0.409 \pm 0.006$	$1.002 \pm 0.001$	$0.993 \pm 0.002$	$4.975 \pm 0.112$	$8.725 \pm 0.206$	$8.968 \pm 0.417$	2.651
2(c)	Peripheral	$\pi^+$	$0.117 \pm 0.004$	$1.099 \pm 0.005$	$0.972 \pm 0.005$	$3.003 \pm 0.098$	$8.335 \pm 0.196$	$10.635 \pm 0.595$	7.995
		$K^+$	$0.173 \pm 0.005$	$1.069 \pm 0.005$	$0.905 \pm 0.006$	$2.375 \pm 0.071$	$7.575 \pm 0.192$	$0.725 \pm 0.043$	1.674
		$p$	$0.263 \pm 0.005$	$1.035 \pm 0.005$	$0.911 \pm 0.006$	$1.875 \pm 0.065$	$7.265 \pm 0.146$	$0.139 \pm 0.009$	2.285
2(d)	Peripheral	$\pi^-$	$0.117 \pm 0.004$	$1.099 \pm 0.005$	$0.972 \pm 0.005$	$3.003 \pm 0.098$	$8.335 \pm 0.196$	$10.635 \pm 0.595$	7.904
		$K^-$	$0.173 \pm 0.005$	$1.069 \pm 0.005$	$0.905 \pm 0.006$	$2.375 \pm 0.071$	$7.575 \pm 0.192$	$0.725 \pm 0.043$	1.875
		$\bar{p}$	$0.263 \pm 0.005$	$1.035 \pm 0.005$	$0.911 \pm 0.006$	$1.875 \pm 0.065$	$7.265 \pm 0.146$	$0.144 \pm 0.009$	2.255

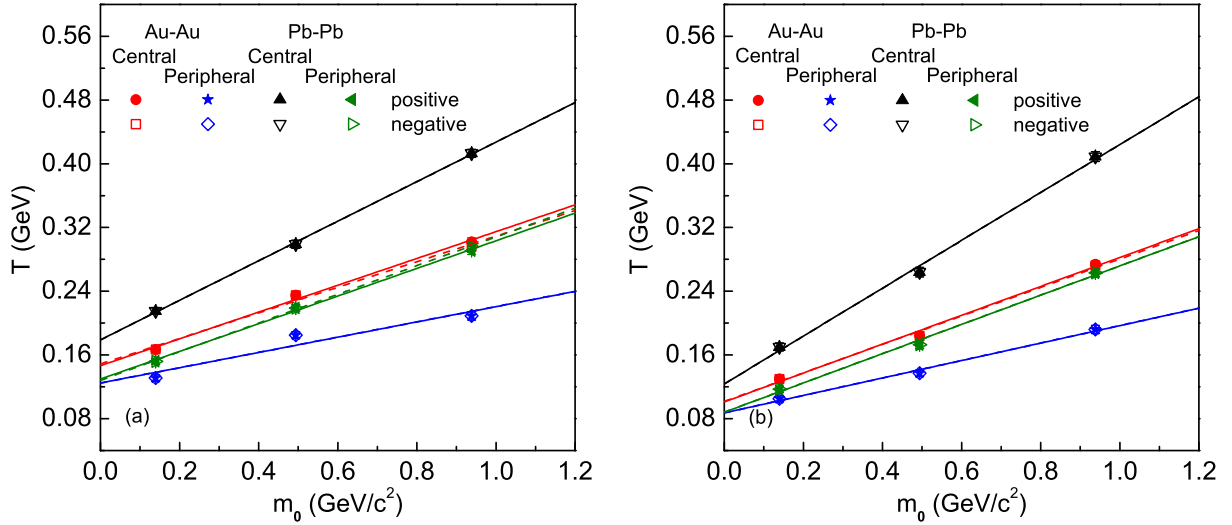


Fig. 3. (Colour figure online) Relations between  $T$  and  $m_0$ . Different symbols represent central (0–5% and 0–12%) and peripheral (80–92% and 60–80%) Au-Au collisions at  $\sqrt{s_{NN}} = 200$  GeV and central (0–5%) and peripheral (80–90% and 60–80%) Pb-Pb collisions at  $\sqrt{s_{NN}} = 2.76$  TeV respectively. The symbols presented in panels (a) and (b) represent the results listed in Tables 4 and 5 and corresponded to the fits of Boltzmann and Tsallis distributions respectively, where the closed and open symbols show the results of positively and negatively charged particles respectively. The solid and dashed lines are the results fitted by the least square method for the positively and negatively charged particles respectively, where the intercepts are regarded as  $T_0$ .

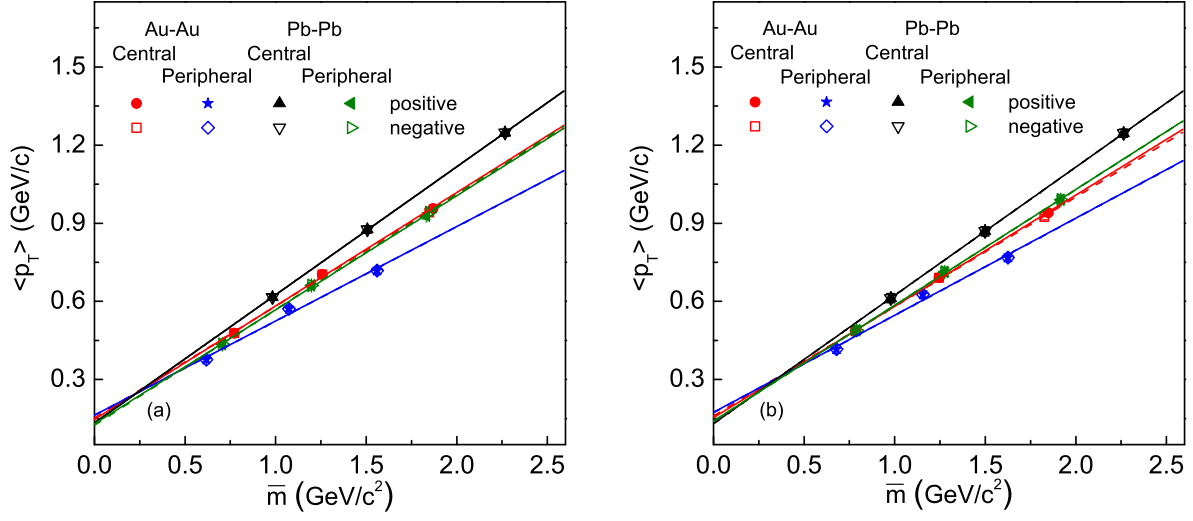


Fig. 4. (Colour figure online) Same as Fig. 3, but showing the relations between  $\langle p_T \rangle$  and  $\overline{m}$ , and the slopes are regarded as  $\beta_T$ . The symbols presented in panels (a) and (b) represent the results obtained according to the fits of Boltzmann and Tsallis distributions respectively, where the values of parameters are listed in Tables 4 and 5 respectively.

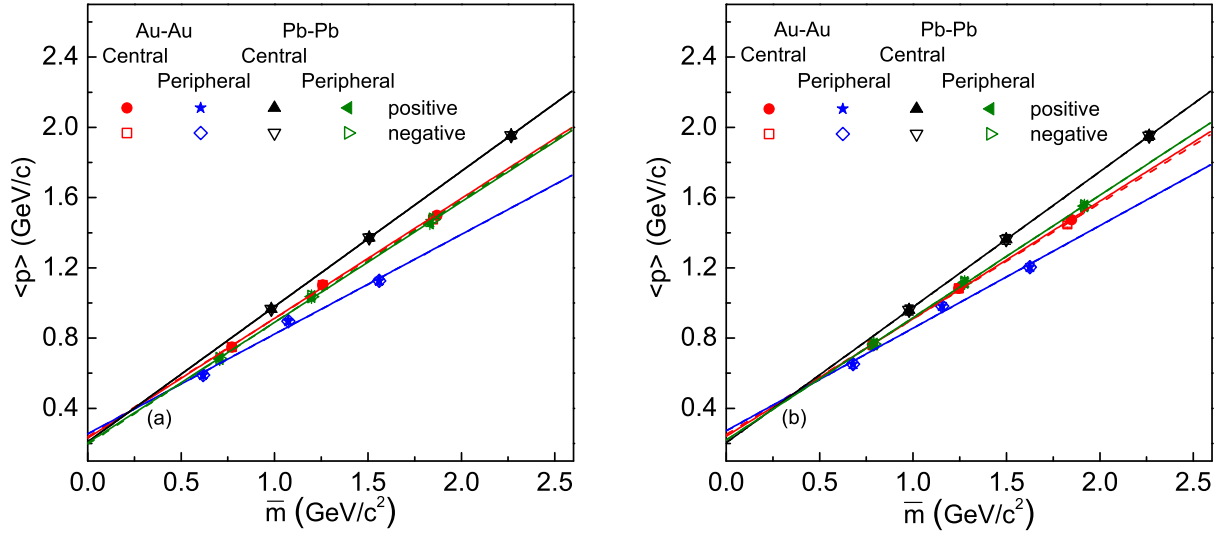


Fig. 5. (Colour figure online) Same as Fig. 3, but showing the relations between  $\langle p \rangle$  and  $\overline{m}$ , and the slopes are regarded as  $\beta$ . The symbols presented in panels (a) and (b) represent the results obtained according to the fits of Boltzmann and Tsallis distributions respectively, where the values of parameters are listed in Tables 4 and 5 respectively.

Table 6. Values of free parameters (intercept and slope) and  $\chi^2/\text{dof}$  corresponding to the relations obtained from the fits of the Boltzmann distribution in Figs. 3(a), 4(a), and 5(a).

Figure	Relation	Type and main particles	Centrality	Intercept	Slope	$\chi^2/\text{dof}$
3(a)	$T - m_0$	Au-Au positive	Central	$0.147 \pm 0.007$	$0.168 \pm 0.012$	2.625
		negative	Central	$0.149 \pm 0.010$	$0.160 \pm 0.016$	4.618
		positive	Peripheral	$0.125 \pm 0.017$	$0.096 \pm 0.028$	14.910
		negative	Peripheral	$0.125 \pm 0.017$	$0.096 \pm 0.028$	14.910
		Pb-Pb positive	Central	$0.179 \pm 0.003$	$0.248 \pm 0.005$	0.424
		negative	Central	$0.179 \pm 0.003$	$0.248 \pm 0.005$	0.424
		positive	Peripheral	$0.130 \pm 0.005$	$0.174 \pm 0.008$	1.142
		negative	Peripheral	$0.128 \pm 0.003$	$0.180 \pm 0.005$	0.394
		4(a)	$\langle p_T \rangle - \bar{m}$	Au-Au positive	Central	$0.147 \pm 0.018$
negative	Central			$0.152 \pm 0.023$	$0.430 \pm 0.017$	1.312
positive	Peripheral			$0.163 \pm 0.041$	$0.362 \pm 0.036$	4.734
negative	Peripheral			$0.163 \pm 0.041$	$0.362 \pm 0.036$	4.734
Pb-Pb positive	Central			$0.133 \pm 0.004$	$0.492 \pm 0.002$	0.024
negative	Central			$0.133 \pm 0.004$	$0.492 \pm 0.002$	0.024
positive	Peripheral			$0.130 \pm 0.013$	$0.438 \pm 0.010$	0.499
negative	Peripheral			$0.125 \pm 0.010$	$0.443 \pm 0.007$	0.285
5(a)	$\langle p \rangle - \bar{m}$			Au-Au positive	Central	$0.230 \pm 0.028$
		negative	Central	$0.239 \pm 0.035$	$0.673 \pm 0.026$	1.313
		positive	Peripheral	$0.255 \pm 0.064$	$0.568 \pm 0.056$	4.746
		negative	Peripheral	$0.255 \pm 0.064$	$0.568 \pm 0.056$	4.746
		Pb-Pb positive	Central	$0.209 \pm 0.006$	$0.771 \pm 0.003$	0.024
		negative	Central	$0.209 \pm 0.006$	$0.771 \pm 0.003$	0.024
		positive	Peripheral	$0.203 \pm 0.020$	$0.686 \pm 0.015$	0.496
		negative	Peripheral	$0.196 \pm 0.015$	$0.694 \pm 0.011$	0.283

Table 7. Values of free parameters (intercept and slope) and  $\chi^2/\text{dof}$  corresponding to the relations obtained from the fits of the Tsallis distribution in Figs. 3(b), 4(b), and 5(b).

Figure	Relation	Type and main particles	Centrality	Intercept	Slope	$\chi^2/\text{dof}$
3(b)	$T - m_0$	Au-Au positive	Central	$0.101 \pm 0.009$	$0.181 \pm 0.014$	3.059
		negative	Central	$0.102 \pm 0.008$	$0.179 \pm 0.013$	2.533
		positive	Peripheral	$0.087 \pm 0.006$	$0.110 \pm 0.009$	1.708
		negative	Peripheral	$0.087 \pm 0.006$	$0.110 \pm 0.009$	1.708
		Pb-Pb positive	Central	$0.124 \pm 0.011$	$0.300 \pm 0.017$	2.877
		negative	Central	$0.124 \pm 0.011$	$0.300 \pm 0.017$	2.877
		positive	Peripheral	$0.088 \pm 0.008$	$0.184 \pm 0.013$	2.258
		negative	Peripheral	$0.088 \pm 0.008$	$0.184 \pm 0.013$	2.258
		4(b)	$\langle p_T \rangle - \bar{m}$	Au-Au positive	Central	$0.154 \pm 0.013$
negative	Central			$0.160 \pm 0.018$	$0.420 \pm 0.013$	0.495
positive	Peripheral			$0.174 \pm 0.049$	$0.373 \pm 0.040$	4.116
negative	Peripheral			$0.174 \pm 0.049$	$0.373 \pm 0.040$	4.116
Pb-Pb positive	Central			$0.131 \pm 0.001$	$0.493 \pm 0.001$	0.001
negative	Central			$0.131 \pm 0.001$	$0.493 \pm 0.001$	0.001
positive	Peripheral			$0.140 \pm 0.011$	$0.445 \pm 0.008$	0.148
negative	Peripheral			$0.140 \pm 0.011$	$0.445 \pm 0.008$	0.148
5(b)	$\langle p \rangle - \bar{m}$			Au-Au positive	Central	$0.240 \pm 0.021$
		negative	Central	$0.251 \pm 0.028$	$0.659 \pm 0.021$	0.494
		positive	Peripheral	$0.272 \pm 0.077$	$0.584 \pm 0.063$	4.111
		negative	Peripheral	$0.272 \pm 0.077$	$0.584 \pm 0.063$	4.111
		Pb-Pb positive	Central	$0.205 \pm 0.002$	$0.772 \pm 0.001$	0.001
		negative	Central	$0.205 \pm 0.002$	$0.772 \pm 0.001$	0.001
		positive	Peripheral	$0.220 \pm 0.017$	$0.697 \pm 0.012$	0.148
		negative	Peripheral	$0.220 \pm 0.017$	$0.697 \pm 0.012$	0.148

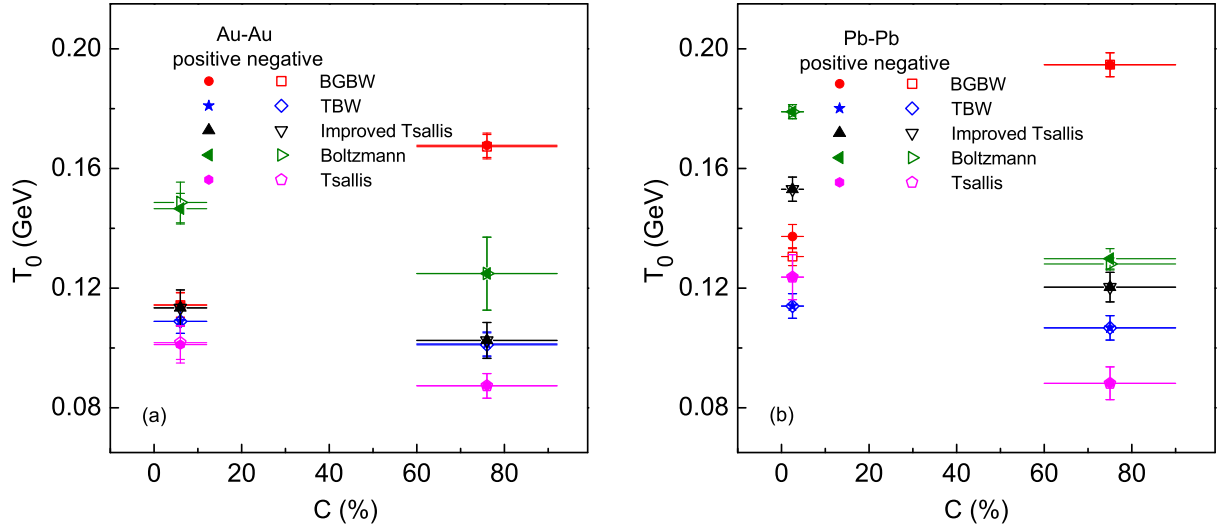


Fig. 6. (Colour figure online) Comparisons of  $T_0$  obtained by different methods for different centralities ( $C$ ), where the values of  $T_0$  in the first three methods are obtained by weighting different particles. Panels (a) and (b) correspond to the results for central (0–5% and 0–12%) and peripheral (80–92% and 60–80%) Au-Au collisions at  $\sqrt{s_{NN}} = 200$  GeV and central (0–5%) and peripheral (80–90% and 60–80%) Pb-Pb collisions at  $\sqrt{s_{NN}} = 2.76$  TeV respectively, where the centralities 0–5% and 0–12%, 80–92% and 60–80%, as well as 80–90% and 60–80% are combined to 0–12%, 60–92%, and 60–90%, respectively.

cases. It is hard to reduce the values of  $\chi^2/\text{dof}$  in our fits.

In the above fits, we have an addition term of inverse power-law to account for hard process. This part contributes a small fraction to the  $p_T$  spectra, though the contribution coverage is wide. In the fitting procedure, according to the changing tendency of data in a low  $p_T$  range from 0 to 2 GeV/ $c$ , the part for soft process can be well constrained first of all, though the contribution of soft process can even reach to 3.5 GeV/ $c$ . Then, the part for hard process can be also constrained conveniently. In addition, in order to give a set of fitted parameters as accurately as possible, we use the least square method in the whole  $p_T$  coverage. It seems that different fitted parameters can be obtained in different  $p_T$  coverages. We should use a  $p_T$  coverage as widely as possible, especially for the extraction of the parameters related to the inverse power-law because that a limited  $p_T$  coverage can not provide a good constrain of the inverse power-law and thus can easily drive the fitted parameters away from their physical meanings. In fact, for extractions of the effective temperature and transverse flow velocity which are the main topics of the present work, a not too wide  $p_T$  coverage such as 0–2~3 GeV/ $c$  is enough due to the soft process contributing only in

the low  $p_T$  region and the changing tendency of data in 0–2 GeV/ $c$  takes part in a main role.

From the above fits one can see that, as a two-component function, Eq. (9) with different soft components can approximately describe the data in a wide  $p_T$  coverage. In addition, in our very recent work [37], we used the method iii) to describe preliminarily the  $p_T$  spectra up to nearly 20 GeV/ $c$ . In our another work [38], two-Boltzmann distribution was used to describe the  $p_T$  spectra up to nearly 14 GeV/ $c$ . Generally, different sets of parameters are needed for different data. In particular, as it is pointed out in Ref. [39], more fitting parameters are needed in order to fit wider  $p_T$  range of particle spectra. In the present work, we fit the particle spectra in a wide  $p_T$  range by introducing the inverse power-law to describe the high  $p_T$  region. The price to pay is 3 more parameters are added. In the two-component function, the contributions of soft and hard components have a little effect in constraining respective free parameters due to different contributive regions, though the contribution fraction of the two components is main role. This results in the  $p_T$  coverage having a small effect on  $T_0$  and  $\beta_T$ . In fact, if we change the boundary of low  $p_T$  region from 2 to 3 or 3.5 GeV/ $c$ , the variations of parameters can be neglected

due to the tendency of curve being mainly determined by the data in 0–2 GeV/ $c$ . Meanwhile, the data in 2–3.5 GeV/ $c$  obey naturally the tendency of curve due to also the contribution or revision of hard component. In other words, because of the revision of hard component, the values of  $T_0$  and  $\beta_T$  are not sensitive to the boundary of low  $p_T$  region. Although different  $p_T$  coverages obtained in different conditions can drive different fitted curves, these differences appear mainly in the high  $p_T$  region and do not largely effect the extraction of  $T_0$  and  $\beta_T$ . In any case, we always use the last square method to extract the fitted parameters. In fact, the method used by us has the minimum randomness in the extractions of the fitted parameters.

It should be noted that although the conventional BGBW and TBW models have only 2–3 parameters to describe the  $p_T$  shape and usually fit several spectra simultaneously to reduce the correlation of the parameters, they seems to cover non-simultaneity of the kinetic freeze-outs of different particles. In the present work, although we use 3 more parameters and fit each spectrum individually, we observe an evidence of the mass dependent differential kinetic freeze-out scenario or multiple kinetic freeze-outs scenario [4, 16, 23]. The larger the temperature (mass) is, the earlier the particle produces. The average temperature (flow velocity and entropy index) of the kinetic freeze-outs for different particles is obtained by weighting different  $T_0$  ( $\beta_T$  and  $q$ ), where the weight factor is the normalization constant of each  $p_T$  spectrum. In the case of using the average temperature (flow velocity and entropy index) to fit the pion, kaon, and proton simultaneously to better constrain the parameters, larger values of  $\chi^2/\text{dof}$  are obtained.

Based on the descriptions of  $p_T$  spectra, the first three methods can give  $T_0$  and  $\beta_T$  conveniently, though the values of parameters are possibly inharmonious due to different methods. In particular, the value of  $T_0$  obtained by the method i) in peripheral collisions is larger than that in central collisions, which is different from the methods ii) and iii) which obtain an opposite result. According to the conventional treatment in refs. [11, 14], the values of  $\beta_T$  obtained by the methods i) and ii) in peripheral collisions are taken to be nearly zero, which are different from the method iii) which obtains a value of about  $0.6c$  in both central and peripheral collisions.

To obtain the values of  $T_0$ ,  $\beta_T$ , and  $\beta$  by the methods iv)<sub>a</sub> and iv)<sub>b</sub>, we analyze the values of  $T$  presented in Tables 4 and 5, and calculate  $\langle p_T \rangle$ ,  $\langle p \rangle$ , and  $\overline{m}$  based

on the values of parameters listed in Tables 4 and 5. In the calculations performed from  $p_T$  to  $\langle p \rangle$  and  $\overline{m}$  by the Monte Carlo method, an isotropic assumption in the rest frame of emission source is used [22–24]. In particular,  $\overline{m}$  is in fact the mean energy  $\langle \sqrt{p^2 + m_0^2} \rangle$ .

The relations between  $T$  and  $m_0$ ,  $\langle p_T \rangle$  and  $\overline{m}$ , as well as  $\langle p \rangle$  and  $\overline{m}$  are shown in Figs. 3, 4, and 5, respectively, where panels (a) and (b) correspond to the methods iv)<sub>a</sub> and iv)<sub>b</sub> which use the Boltzmann and Tsallis distributions respectively. Different symbols represent central (0–5% and 0–12%) and peripheral (80–92% and 60–80%) Au-Au collisions at  $\sqrt{s_{NN}} = 200$  GeV and central (0–5%) and peripheral (80–90% and 60–80%) Pb-Pb collisions at  $\sqrt{s_{NN}} = 2.76$  TeV respectively, where the centralities 0–5% and 0–12%, 80–92% and 60–80%, as well as 80–90% and 60–80% can be combined to 0–12%, 60–92%, and 60–90%, respectively. The symbols in Fig. 3 represent values of  $T$  listed in Tables 4 and 5 for different  $m_0$ . The symbols in Figs. 4 and 5 represent values of  $\langle p_T \rangle$  and  $\langle p \rangle$  for different  $\overline{m}$  respectively, which are calculated due to the parameters listed in Tables 4 and 5 and the isotropic assumption in the rest frame of emission source. The solid and dashed lines in the three figures are the results fitted by the least square method for the positively and negatively charged particles respectively. The values of intercepts, slopes, and  $\chi^2/\text{dof}$  are listed in Tables 6 and 7 which correspond to the methods iv)<sub>a</sub> and iv)<sub>b</sub> respectively. One can see that, in most cases, the mentioned relations are described by a linear function. In particular, the intercept in Fig. 3 is regarded as  $T_0$ , and the slopes in Figs. 4 and 5 are regarded as  $\beta_T$  and  $\beta$  respectively. The values of  $T$ ,  $T_0$ ,  $\beta_T$ ,  $\beta$ , and  $\overline{m}$  are approximately independent of isospin.

To compare values of key parameters obtained by different methods for different centralities (both central and peripheral collisions), Figs. 6 and 7 show  $T_0$  and  $\beta_T$  respectively, where panels (a) and (b) correspond to the results for central (0–5% and 0–12%) and peripheral (80–92% and 60–80%) Au-Au collisions at  $\sqrt{s_{NN}} = 200$  GeV and central (0–5%) and peripheral (80–90% and 60–80%) Pb-Pb collisions at  $\sqrt{s_{NN}} = 2.76$  TeV respectively. The closed and open symbols represent positively and negatively charged particles respectively, which are quoted from Tables 1, 2, 3, 6, and 7 which correspond to the methods i), ii), iii), iv)<sub>a</sub>, and iv)<sub>b</sub>, respectively. In particular, the values of  $T_0$  and  $\beta_T$  in the first three methods are obtained by weighting different particles. One can see that, by using the method i), the value of

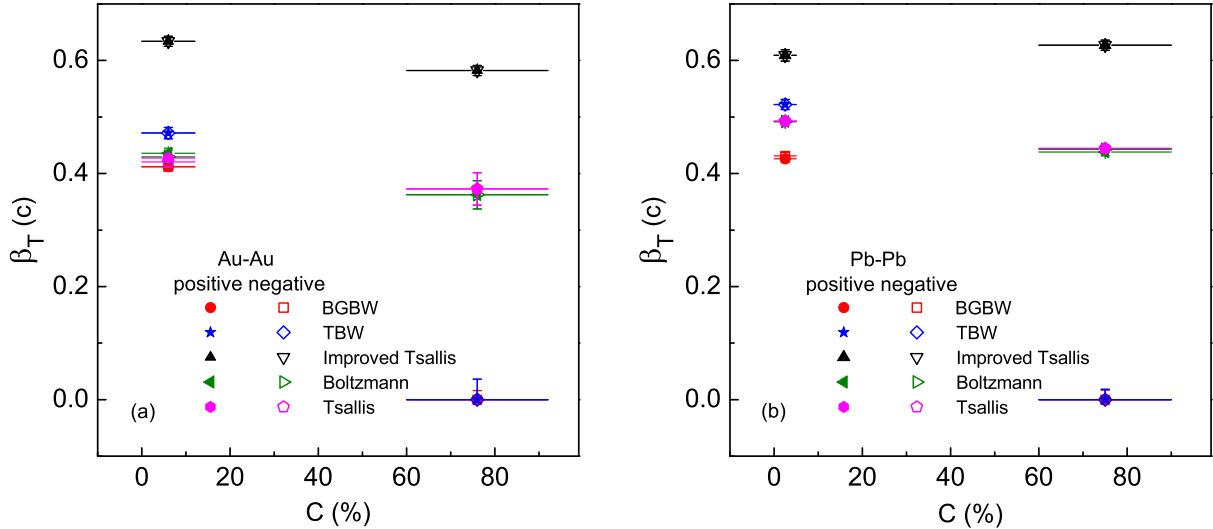


Fig. 7. (Colour figure online) Same as Fig. 6, but showing the comparisons of  $\beta_T$  obtained by different methods for different centralities.

$T_0$  in central collisions is smaller than that in peripheral collisions, and other methods present a larger  $T_0$  in central collisions. The methods i) and ii) show a nearly zero  $\beta_T$  in peripheral collisions according to refs. [11, 14], while other methods show a considerable  $\beta_T$  in both central and peripheral collisions.

To explain the inconsistent results in  $T_0$  and  $\beta_T$  for different methods, we re-examine the first two methods. It should be noticed that the same flow profile function,  $\beta(r) = \beta_S(r/R)^{n_0}$ , and the same transverse flow velocity,  $\beta_T = 2\beta_S/(n_0+2)$ , are used in the first two methods, though  $n_0 = 2$  is used in the method i) [11] and  $n_0 = 1$  is used in the method ii) [14] with the conventional treatment. As an insensitive quantity, although the radial size  $R$  of the thermal source in central collisions can be approximately regarded as the radius of a collision nucleus, and in peripheral collisions  $R$  is not zero due to a few participant nucleons taking part in the interactions in which we can take approximately  $R$  to be 2.5 fm, both the methods i) and ii) use a nearly zero  $\beta_T$  in peripheral collisions [11, 14]. If we consider a non-zero  $\beta_T$  in peripheral collisions for the methods i) and ii), the situation will be changed.

By using a non-zero  $\beta_T$  in peripheral collisions for the methods i) and ii), we re-analyze the data presented in Figs. 1 and 2. At the same time, to see the influences of different  $n_0$  in the self-similar flow profile, we refit the mentioned  $p_T$  spectra by the first two methods with

$n_0 = 1$  and 2 synchronously. The results re-analyzed by us are shown in Figs. 8 and 9 which correspond to 200 GeV Au-Au and 2.76 TeV Pb-Pb collisions respectively. The data points are the same as Figs. 1 and 2 [25–29]. The dotted, solid, dashed, and dotted-dashed curves correspond to the results of the method i) with  $n_0 = 1$  and 2, and of the method ii) with  $n_0 = 1$  and 2, respectively, where the results of the method i) with  $n_0 = 2$  and of the method ii) with  $n_0 = 1$  in central collisions are the same as Figs. 1 and 2. The values of related parameters and  $\chi^2/\text{dof}$  are listed in Tables 8 and 9, where the parameters for the method i) with  $n_0 = 2$  and for the method ii) with  $n_0 = 1$  in central collisions repeat those in Tables 1 and 2, which are not listed again. One can see that, after the re-examination, the values of  $T_0$  in central collisions are larger than those in peripheral collisions. The values of  $\beta_T$  in peripheral collisions are no longer zero. These new results are consistent with other methods.

To give new comparisons for  $T_0$  and  $\beta_T$ , the new results obtained by the first two methods are shown in Figs. 10 and 11 respectively, where the results corresponding to the method i) for central collisions with  $n_0 = 2$  and to the method ii) for central collisions with  $n_0 = 1$  are the same as those in Figs. 6 and 7. Combining Figs. 6, 7, 10, and 11, one can see that the four methods show approximately the consistent results. These comparisons enlighten us to use the first two methods

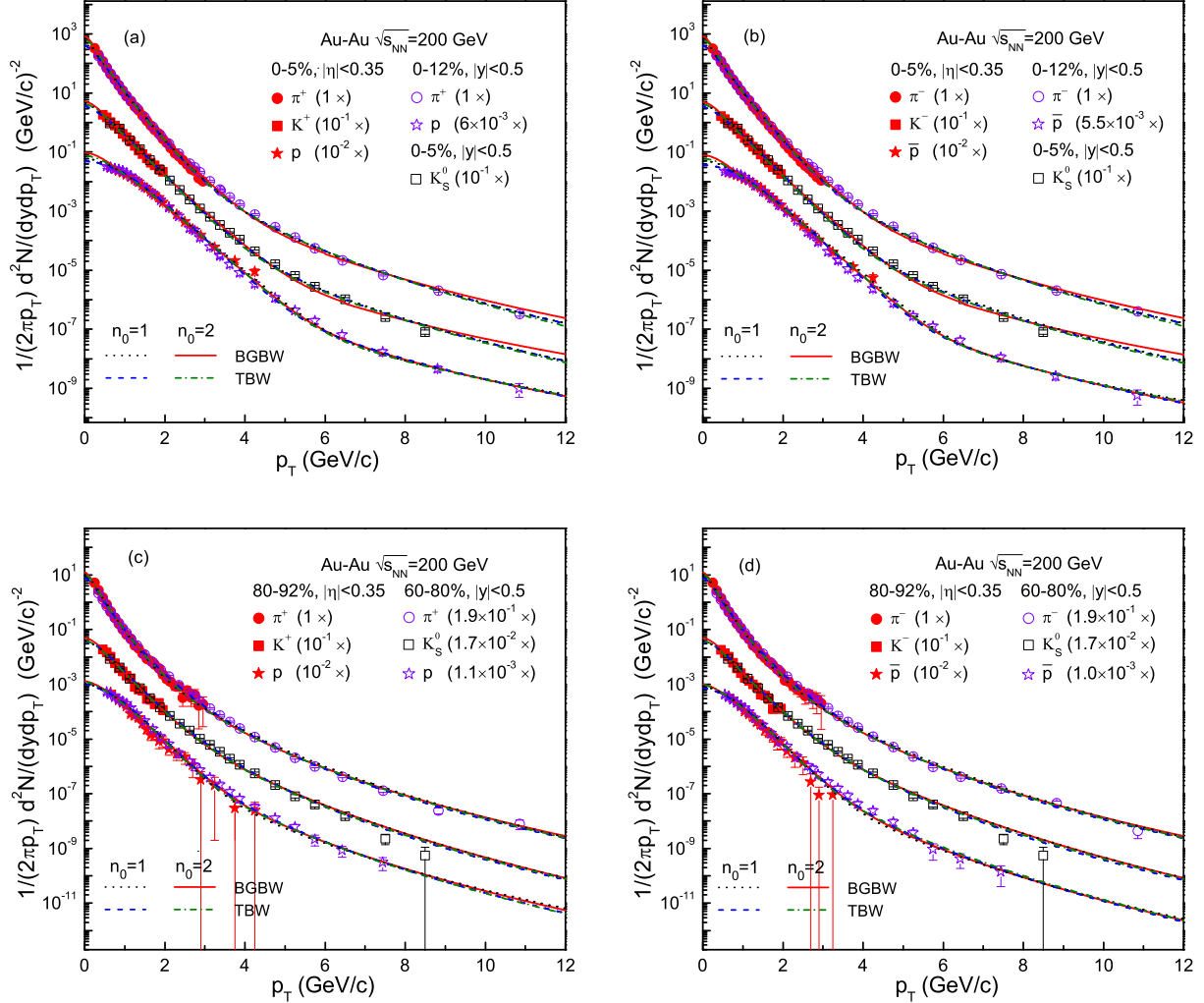


Fig. 8. (Colour figure online) Reanalyzing the transverse momentum spectra [25–27] collected in Fig. 1 by the first two methods. The dotted, solid, dashed, and dotted-dashed curves are our results calculated by using the method i) with  $n_0 = 1$  and 2, as well as the method ii) with  $n_0 = 1$  and 2, respectively. The results for central collisions obtained by the method i) with  $n_0 = 2$  and by the method ii) with  $n_0 = 1$  are the same as Fig. 1.

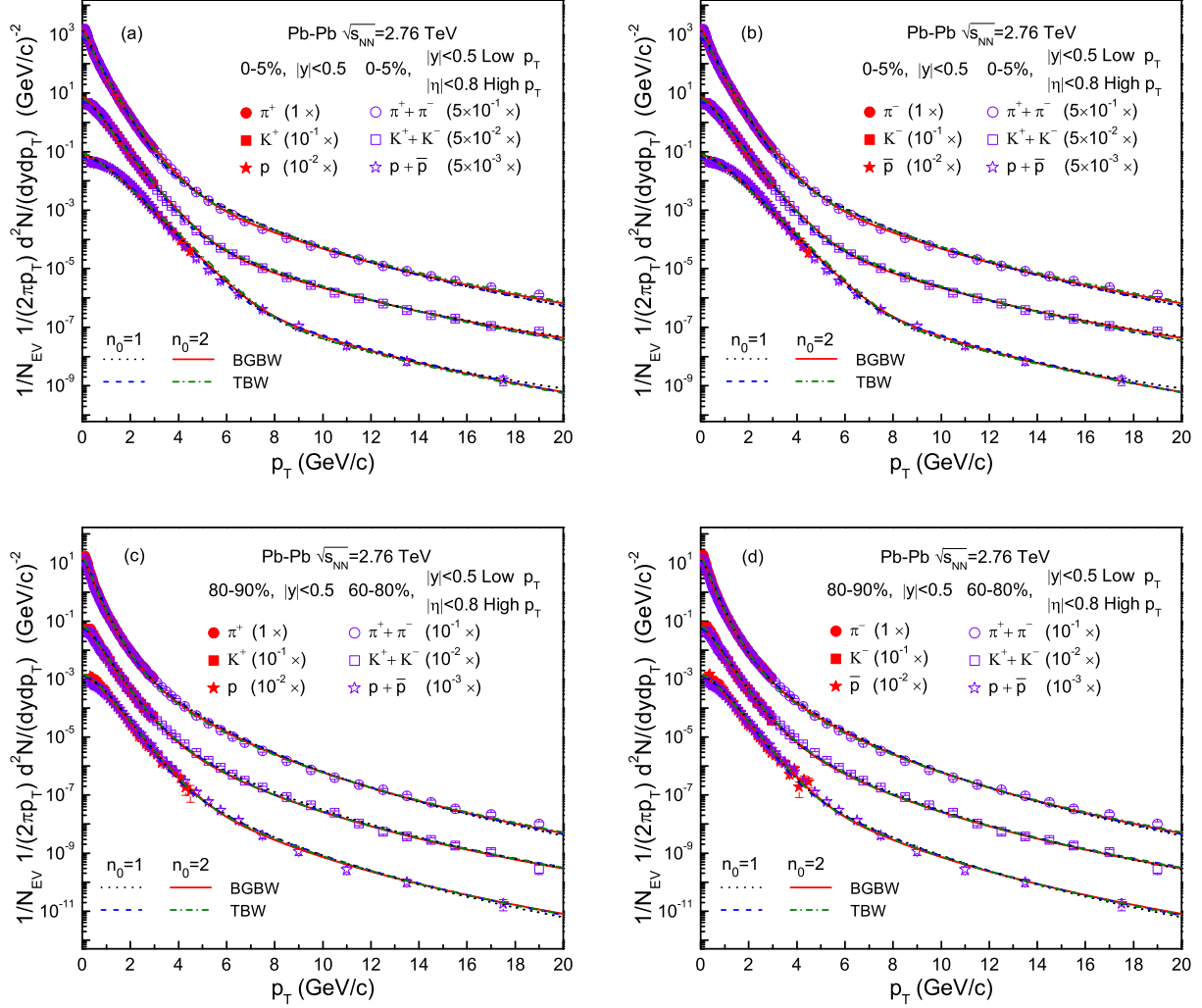


Fig. 9. (Colour figure online) Same as Fig. 8, but reanalyzing the transverse momentum spectra [28, 29] collected in Fig. 2 by the first two methods. The results for central collisions obtained by the method i) with  $n_0 = 2$  and by the method ii) with  $n_0 = 1$  are the same as Fig. 2.



Table 8. Values of free parameters ( $T_0$ ,  $\beta_T$ ,  $k$ ,  $p_0$ , and  $n$ ), normalization constant ( $N_0$ ), and  $\chi^2/\text{dof}$  corresponding to the fits of method i) in Figs. 8 and 9, where the values for central collisions with  $n_0 = 2$  in the self-similar flow profile repeat those in Table 1, which are not listed again.

Fig.	Cent.	Main Part.	$T_0$ (GeV)	$\beta_T$ (c)	$k$	$p_0$ (GeV/c)	$n$	$N_0$	$\chi^2/\text{dof}$
8(a)	Central	$\pi^+$	$0.138 \pm 0.005$	$0.452 \pm 0.008$	$0.964 \pm 0.006$	$2.375 \pm 0.069$	$10.365 \pm 0.188$	$633.869 \pm 62.976$	3.369
Au-Au $n_0 = 1$	Central	$K^+$	$0.169 \pm 0.005$	$0.412 \pm 0.008$	$0.901 \pm 0.006$	$1.998 \pm 0.058$	$9.675 \pm 0.185$	$54.966 \pm 3.838$	5.502
		$p$	$0.198 \pm 0.005$	$0.398 \pm 0.008$	$0.995 \pm 0.002$	$2.485 \pm 0.072$	$8.075 \pm 0.171$	$8.457 \pm 0.646$	5.274
		$\pi^-$	$0.138 \pm 0.005$	$0.452 \pm 0.008$	$0.964 \pm 0.006$	$2.375 \pm 0.069$	$10.365 \pm 0.188$	$633.869 \pm 62.976$	3.277
8(b)	Central	$K^-$	$0.169 \pm 0.005$	$0.412 \pm 0.008$	$0.901 \pm 0.006$	$2.098 \pm 0.060$	$9.835 \pm 0.188$	$54.759 \pm 3.823$	6.405
8(c)	Peripheral	$\bar{p}$	$0.198 \pm 0.005$	$0.397 \pm 0.008$	$0.994 \pm 0.002$	$2.185 \pm 0.070$	$7.975 \pm 0.168$	$7.096 \pm 0.649$	12.058
		$\pi^+$	$0.115 \pm 0.005$	$0.415 \pm 0.008$	$0.901 \pm 0.008$	$2.512 \pm 0.079$	$11.123 \pm 0.173$	$11.713 \pm 0.591$	4.455
		$K^+$	$0.145 \pm 0.005$	$0.415 \pm 0.008$	$0.888 \pm 0.008$	$3.923 \pm 0.082$	$12.923 \pm 0.178$	$0.482 \pm 0.077$	6.711
8(d)	Peripheral	$p$	$0.157 \pm 0.006$	$0.353 \pm 0.008$	$0.947 \pm 0.008$	$3.316 \pm 0.069$	$11.016 \pm 0.169$	$0.142 \pm 0.015$	1.444
		$\pi^-$	$0.115 \pm 0.005$	$0.415 \pm 0.008$	$0.901 \pm 0.008$	$2.512 \pm 0.079$	$11.123 \pm 0.173$	$11.713 \pm 0.591$	3.800
		$K^-$	$0.145 \pm 0.005$	$0.415 \pm 0.008$	$0.888 \pm 0.008$	$3.923 \pm 0.082$	$12.923 \pm 0.178$	$0.482 \pm 0.077$	5.907
8(c)	Peripheral	$\bar{p}$	$0.157 \pm 0.006$	$0.353 \pm 0.008$	$0.945 \pm 0.008$	$3.316 \pm 0.069$	$11.528 \pm 0.169$	$0.112 \pm 0.011$	0.904
Au-Au $n_0 = 2$	Peripheral	$\pi^+$	$0.103 \pm 0.005$	$0.395 \pm 0.008$	$0.896 \pm 0.008$	$2.012 \pm 0.063$	$10.203 \pm 0.185$	$14.240 \pm 1.308$	2.956
		$K^+$	$0.117 \pm 0.006$	$0.383 \pm 0.008$	$0.901 \pm 0.008$	$3.983 \pm 0.071$	$12.993 \pm 0.195$	$0.636 \pm 0.033$	4.221
		$p$	$0.118 \pm 0.006$	$0.355 \pm 0.008$	$0.905 \pm 0.006$	$3.268 \pm 0.066$	$11.506 \pm 0.186$	$0.170 \pm 0.012$	1.093
8(d)	Peripheral	$\pi^-$	$0.103 \pm 0.005$	$0.395 \pm 0.008$	$0.896 \pm 0.008$	$2.012 \pm 0.063$	$10.203 \pm 0.185$	$14.240 \pm 1.308$	2.652
9(a)	Central	$K^-$	$0.117 \pm 0.006$	$0.383 \pm 0.008$	$0.901 \pm 0.008$	$3.983 \pm 0.071$	$12.993 \pm 0.195$	$0.636 \pm 0.033$	3.879
		$\bar{p}$	$0.118 \pm 0.006$	$0.355 \pm 0.008$	$0.905 \pm 0.006$	$3.268 \pm 0.066$	$11.926 \pm 0.186$	$0.128 \pm 0.012$	0.589
		$\pi^+$	$0.149 \pm 0.005$	$0.473 \pm 0.008$	$0.922 \pm 0.008$	$1.535 \pm 0.056$	$7.276 \pm 0.104$	$1465.409 \pm 127.197$	3.815
Pb-Pb $n_0 = 1$	Central	$K^+$	$0.235 \pm 0.005$	$0.399 \pm 0.008$	$0.938 \pm 0.008$	$1.295 \pm 0.055$	$6.114 \pm 0.101$	$77.086 \pm 7.666$	1.463
		$p$	$0.338 \pm 0.005$	$0.332 \pm 0.006$	$0.991 \pm 0.002$	$2.285 \pm 0.082$	$6.485 \pm 0.108$	$10.152 \pm 0.330$	11.411
		$\pi^-$	$0.149 \pm 0.005$	$0.473 \pm 0.008$	$0.922 \pm 0.008$	$1.535 \pm 0.056$	$7.276 \pm 0.104$	$1465.409 \pm 127.197$	3.751
9(b)	Central	$K^-$	$0.235 \pm 0.005$	$0.399 \pm 0.008$	$0.938 \pm 0.008$	$1.295 \pm 0.055$	$6.114 \pm 0.101$	$77.157 \pm 7.674$	1.229
9(c)	Peripheral	$\bar{p}$	$0.338 \pm 0.005$	$0.332 \pm 0.006$	$0.991 \pm 0.002$	$2.285 \pm 0.082$	$6.485 \pm 0.108$	$10.152 \pm 0.330$	10.234
		$\pi^+$	$0.127 \pm 0.005$	$0.473 \pm 0.008$	$0.934 \pm 0.008$	$2.793 \pm 0.078$	$8.765 \pm 0.138$	$14.233 \pm 0.756$	8.290
		$K^+$	$0.169 \pm 0.004$	$0.453 \pm 0.008$	$0.902 \pm 0.008$	$2.665 \pm 0.074$	$7.995 \pm 0.129$	$0.723 \pm 0.050$	2.448
9(d)	Peripheral	$p$	$0.180 \pm 0.005$	$0.436 \pm 0.008$	$0.918 \pm 0.008$	$2.995 \pm 0.092$	$8.599 \pm 0.132$	$0.167 \pm 0.014$	3.944
		$\pi^-$	$0.127 \pm 0.005$	$0.473 \pm 0.008$	$0.934 \pm 0.008$	$2.793 \pm 0.078$	$8.765 \pm 0.138$	$14.233 \pm 0.756$	8.285
		$K^-$	$0.169 \pm 0.004$	$0.453 \pm 0.008$	$0.902 \pm 0.008$	$2.665 \pm 0.074$	$7.995 \pm 0.129$	$0.723 \pm 0.050$	2.686
9(c)	Peripheral	$\bar{p}$	$0.180 \pm 0.005$	$0.436 \pm 0.008$	$0.918 \pm 0.008$	$2.995 \pm 0.092$	$8.599 \pm 0.132$	$0.167 \pm 0.014$	4.196
Pb-Pb $n_0 = 2$	Peripheral	$\pi^+$	$0.116 \pm 0.004$	$0.410 \pm 0.008$	$0.941 \pm 0.007$	$2.393 \pm 0.058$	$8.185 \pm 0.153$	$17.976 \pm 0.731$	4.533
		$K^+$	$0.184 \pm 0.005$	$0.367 \pm 0.008$	$0.908 \pm 0.007$	$2.375 \pm 0.056$	$7.585 \pm 0.145$	$0.702 \pm 0.044$	1.120
		$p$	$0.204 \pm 0.005$	$0.343 \pm 0.008$	$0.919 \pm 0.007$	$2.178 \pm 0.055$	$7.515 \pm 0.145$	$0.172 \pm 0.015$	1.791
9(d)	Peripheral	$\pi^-$	$0.116 \pm 0.004$	$0.410 \pm 0.008$	$0.941 \pm 0.007$	$2.393 \pm 0.058$	$8.185 \pm 0.153$	$17.976 \pm 0.731$	4.601
9(d)	Peripheral	$K^-$	$0.184 \pm 0.005$	$0.367 \pm 0.008$	$0.908 \pm 0.007$	$2.375 \pm 0.056$	$7.585 \pm 0.145$	$0.702 \pm 0.044$	1.232
		$\bar{p}$	$0.204 \pm 0.005$	$0.343 \pm 0.008$	$0.919 \pm 0.007$	$2.178 \pm 0.055$	$7.515 \pm 0.145$	$0.172 \pm 0.015$	1.963

Table 9. Values of free parameters ( $T_0$ ,  $q$ ,  $\beta_T$ ,  $k$ ,  $p_0$ , and  $n$ ), normalization constant ( $N_0$ ), and  $\chi^2/\text{dof}$  corresponding to the fits of method ii) in Figs. 8 and 9, where the values for central collisions with  $n_0 = 1$  in the self-similar flow profile repeat those in Table 2, which are not listed again.

Fig.	Cent.	Main Part.	$T_0$ (GeV)	$q$	$\beta_T$ (c)	$k$	$p_0$ (GeV/c)	$n$	$N_0$	$\chi^2/\text{dof}$
8(c)	Peripheral	$\pi^+$	$0.079 \pm 0.004$	$1.069 \pm 0.006$	$0.405 \pm 0.009$	$0.924 \pm 0.006$	$2.192 \pm 0.083$	$10.379 \pm 0.189$	$9.197 \pm 0.912$	1.715
Au-Au $n_0 = 1$	Peripheral	$K^+$	$0.089 \pm 0.005$	$1.063 \pm 0.005$	$0.389 \pm 0.009$	$0.921 \pm 0.006$	$3.602 \pm 0.096$	$12.282 \pm 0.165$	$0.491 \pm 0.052$	4.499
		$p$	$0.095 \pm 0.005$	$1.028 \pm 0.005$	$0.389 \pm 0.009$	$0.902 \pm 0.007$	$3.810 \pm 0.102$	$12.568 \pm 0.171$	$0.134 \pm 0.010$	1.457
		$\pi^-$	$0.079 \pm 0.004$	$1.069 \pm 0.006$	$0.405 \pm 0.009$	$0.924 \pm 0.006$	$2.192 \pm 0.083$	$10.379 \pm 0.189$	$9.197 \pm 0.912$	1.445
8(d)	Peripheral	$K^-$	$0.089 \pm 0.005$	$1.061 \pm 0.005$	$0.389 \pm 0.009$	$0.921 \pm 0.006$	$3.602 \pm 0.096$	$12.282 \pm 0.165$	$0.486 \pm 0.052$	3.127
8(a)	Central	$\bar{p}$	$0.095 \pm 0.005$	$1.028 \pm 0.005$	$0.389 \pm 0.009$	$0.908 \pm 0.007$	$3.810 \pm 0.102$	$12.868 \pm 0.171$	$0.100 \pm 0.010$	0.670
		$\pi^+$	$0.091 \pm 0.003$	$1.010 \pm 0.005$	$0.401 \pm 0.008$	$0.985 \pm 0.003$	$3.591 \pm 0.091$	$12.035 \pm 0.173$	$683.617 \pm 48.090$	3.630
		$K^+$	$0.103 \pm 0.005$	$1.008 \pm 0.004$	$0.395 \pm 0.007$	$0.961 \pm 0.004$	$2.675 \pm 0.103$	$10.327 \pm 0.089$	$51.119 \pm 5.034$	5.703
Au-Au $n_0 = 2$	Central	$p$	$0.118 \pm 0.005$	$1.009 \pm 0.004$	$0.374 \pm 0.005$	$0.997 \pm 0.002$	$3.385 \pm 0.168$	$8.895 \pm 0.108$	$9.706 \pm 0.421$	6.866
		$\pi^-$	$0.091 \pm 0.003$	$1.010 \pm 0.005$	$0.401 \pm 0.008$	$0.985 \pm 0.003$	$3.591 \pm 0.091$	$12.035 \pm 0.173$	$683.617 \pm 48.090$	3.362
		$K^-$	$0.103 \pm 0.005$	$1.008 \pm 0.004$	$0.395 \pm 0.007$	$0.961 \pm 0.004$	$2.675 \pm 0.103$	$10.327 \pm 0.159$	$49.059 \pm 5.034$	6.731
8(b)	Central	$\bar{p}$	$0.118 \pm 0.005$	$1.009 \pm 0.004$	$0.374 \pm 0.005$	$0.997 \pm 0.002$	$3.385 \pm 0.168$	$9.095 \pm 0.112$	$7.862 \pm 0.422$	15.669
		$\pi^+$	$0.073 \pm 0.004$	$1.025 \pm 0.004$	$0.398 \pm 0.008$	$0.943 \pm 0.004$	$2.653 \pm 0.091$	$11.093 \pm 0.169$	$10.627 \pm 0.888$	3.602
		$K^+$	$0.082 \pm 0.005$	$1.033 \pm 0.005$	$0.380 \pm 0.008$	$0.891 \pm 0.005$	$3.683 \pm 0.092$	$12.553 \pm 0.170$	$0.470 \pm 0.005$	4.498
8(c)	Peripheral	$p$	$0.085 \pm 0.005$	$1.009 \pm 0.005$	$0.359 \pm 0.008$	$0.910 \pm 0.005$	$3.950 \pm 0.093$	$12.756 \pm 0.181$	$0.150 \pm 0.013$	1.306
		$\pi^-$	$0.073 \pm 0.004$	$1.025 \pm 0.004$	$0.398 \pm 0.008$	$0.943 \pm 0.004$	$2.653 \pm 0.091$	$11.093 \pm 0.169$	$10.627 \pm 0.888$	3.239
		$K^-$	$0.082 \pm 0.005$	$1.033 \pm 0.005$	$0.380 \pm 0.008$	$0.891 \pm 0.005$	$3.683 \pm 0.092$	$12.553 \pm 0.170$	$0.470 \pm 0.052$	3.570
8(d)	Peripheral	$\bar{p}$	$0.085 \pm 0.005$	$1.009 \pm 0.005$	$0.359 \pm 0.008$	$0.910 \pm 0.005$	$3.950 \pm 0.093$	$13.018 \pm 0.181$	$0.117 \pm 0.011$	0.647
9(c)	Peripheral	$\pi^+$	$0.089 \pm 0.004$	$1.041 \pm 0.005$	$0.446 \pm 0.010$	$0.929 \pm 0.006$	$2.403 \pm 0.075$	$8.398 \pm 0.169$	$14.318 \pm 0.567$	12.971
Pb-Pb $n_0 = 1$	Peripheral	$K^+$	$0.099 \pm 0.005$	$1.065 \pm 0.005$	$0.446 \pm 0.010$	$0.926 \pm 0.006$	$2.375 \pm 0.071$	$7.468 \pm 0.153$	$0.650 \pm 0.062$	1.544
		$p$	$0.110 \pm 0.005$	$1.030 \pm 0.005$	$0.446 \pm 0.010$	$0.894 \pm 0.007$	$2.415 \pm 0.077$	$8.005 \pm 0.161$	$0.157 \pm 0.014$	2.881
		$\pi^-$	$0.089 \pm 0.004$	$1.041 \pm 0.005$	$0.446 \pm 0.010$	$0.929 \pm 0.006$	$2.403 \pm 0.075$	$8.398 \pm 0.169$	$14.318 \pm 0.567$	12.947
9(d)	Peripheral	$K^-$	$0.099 \pm 0.005$	$1.065 \pm 0.005$	$0.446 \pm 0.010$	$0.926 \pm 0.006$	$2.375 \pm 0.071$	$7.468 \pm 0.153$	$0.650 \pm 0.062$	1.724
9(a)	Central	$\bar{p}$	$0.110 \pm 0.005$	$1.030 \pm 0.005$	$0.446 \pm 0.010$	$0.894 \pm 0.007$	$2.415 \pm 0.077$	$8.005 \pm 0.161$	$0.157 \pm 0.014$	3.065
		$\pi^+$	$0.099 \pm 0.005$	$1.006 \pm 0.004$	$0.435 \pm 0.006$	$0.989 \pm 0.003$	$2.775 \pm 0.085$	$7.515 \pm 0.158$	$1099.140 \pm 107.121$	2.897
		$K^+$	$0.113 \pm 0.005$	$1.002 \pm 0.001$	$0.435 \pm 0.006$	$0.984 \pm 0.003$	$3.575 \pm 0.101$	$7.735 \pm 0.115$	$73.563 \pm 7.358$	3.623

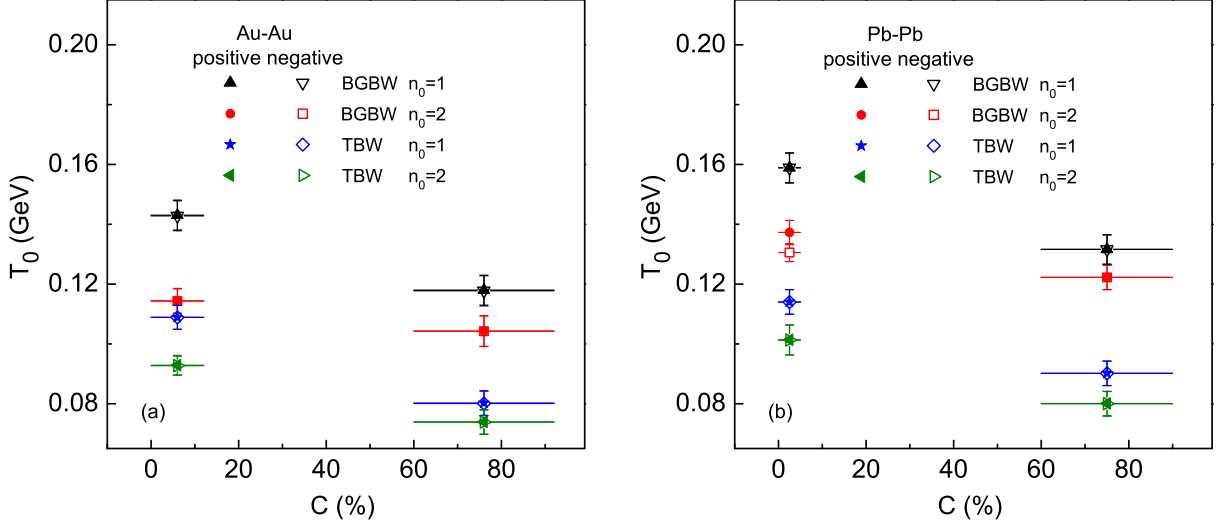


Fig. 10. (Colour figure online) Comparisons of  $T_0$  obtained by the first two methods with  $n_0 = 1$  and 2 for different centralities. Panels (a) and (b) correspond to the results for central (0–5% and 0–12%) and peripheral (80–92% and 60–80%) Au-Au collisions at  $\sqrt{s_{NN}} = 200$  GeV and central (0–5%) and peripheral (80–90% and 60–80%) Pb-Pb collisions at  $\sqrt{s_{NN}} = 2.76$  TeV respectively. The values of  $T_0$  are obtained by weighting different particles and the results for central collisions obtained by the method i) with  $n_0 = 2$  and by the method ii) with  $n_0 = 1$  are the same as Fig. 6.

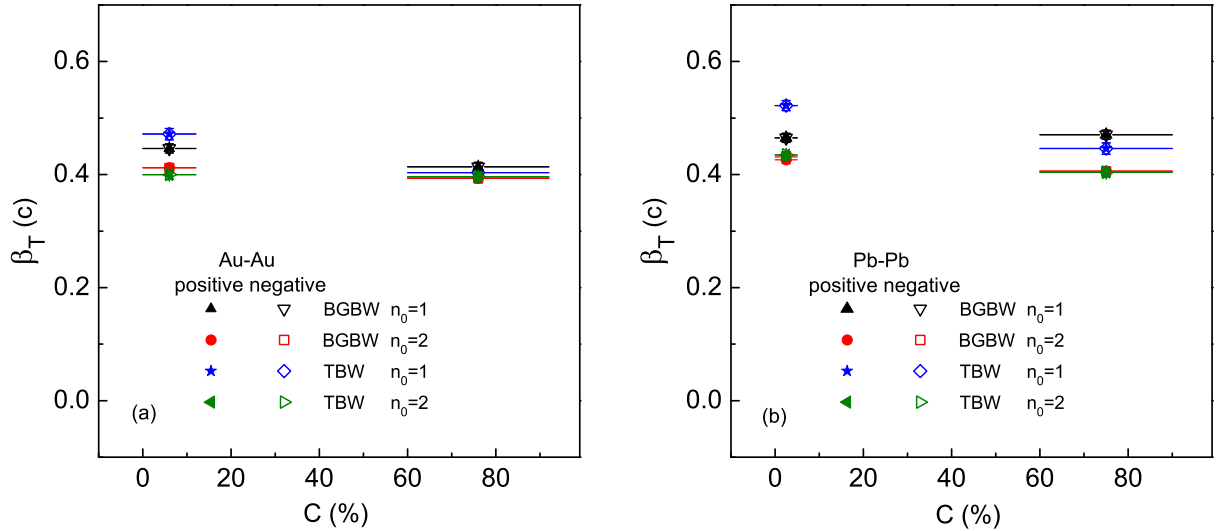


Fig. 11. (Colour figure online) Same as Fig. 10, but showing the comparisons of  $\beta_T$  obtained by the first two methods for different centralities. The results for central collisions obtained by the method i) with  $n_0 = 2$  and by the method ii) with  $n_0 = 1$  are the same as Fig. 7.

in peripheral collisions by a non-zero  $\beta_T$ . After the re-examination for  $\beta_T$  in peripheral collisions, we obtain a relative larger  $T_0$  in central collisions for the four methods. In particular, the parameter  $T_0$  at the LHC is slightly larger than or nearly equal to that at the RHIC, not only for central collisions but also for peripheral collisions. Except the method iii), other methods show a slightly larger or nearly invariant  $\beta_T$  in central collisions comparing with peripheral collisions, and at the LHC comparing with the RHIC, while the method iii) shows a nearly the same  $\beta_T$  in different centralities and at different energies.

We would like to point out that, in the re-examination for  $\beta_T$  in the methods i) and ii), we have assumed both  $\beta_T$  in central and peripheral collisions to be non-zero. While, in most cases [11, 14], both the conventional BGBW and TBW models used non-zero  $\beta_T$  in central collisions and zero (or almost zero)  $\beta_T$  in peripheral collisions. In the case of using a non-zero or zero (or almost zero)  $\beta_T$  in peripheral collisions, we can obtain a relatively smaller or larger  $T_0$ , comparing with central collisions. Indeed, the selection of  $\beta_T$  in peripheral collisions is an important issue in both the BGBW and TBW models. In fact,  $\beta_T$  is a sensitive quantity which can affect  $T_0$ . The larger  $\beta_T$  is selected, the smaller  $T_0$  is needed. The main correlation is between  $\beta_T$  and  $T_0$ , and the effect of  $n_0$  is very small. In Figs. 1 and 2, we have used a zero  $\beta_T$  for peripheral collisions and obtained a harmonious result on relative size of  $T_0$  with Ref. [28] in which  $\beta_T$  ( $0.35c$ ) for peripheral collisions is nearly a half of that ( $0.65c$ ) for central collisions, and  $n_0$  is also different from ours. While in Figs. 8 and 9, we have used a non-zero and slightly smaller  $\beta_T$  for peripheral collisions and obtained a different result from Ref. [28].

In order to make the conclusion more convincing, we can only fit the low  $p_T$  region of the particle spectra using the four methods with the same  $p_T$  cut to decrease the number of free fitting parameters. When the  $p_T$  cut increases from 2 to 3.5 GeV/ $c$ ,  $T_0$  (or  $T$ ) increases or both  $T_0$  (or  $T$ ) and  $\beta_T$  increase slightly. The relative size of  $T_0$  ( $\beta_T$ ) obtained above for central and peripheral collisions is unchanged. In particular,  $\beta_T$  is also a sensitive quantity. For peripheral collisions, a zero or non-zero  $\beta_T$  in the first two methods can give different results. In our opinion, in central and peripheral collisions, it depends on  $\beta_T$  if we want to determine which  $T_0$  is larger. We are inclined to use a non-zero  $\beta_T$  for peripheral collisions due to small system which is similar to

peripheral collisions in number of participant nucleons also showing collective expansion [40].

Comparing with peripheral collisions, the larger  $T_0$  in central collisions renders more deposition of collision energy and higher excitation of interacting system due to more participant nucleons taking part in the violent collisions. Comparing with the top RHIC energy, the larger  $T_0$  at the LHC energy also renders more deposition of collision energy and higher excitation of interacting system due to higher  $\sqrt{s_{NN}}$  at the LHC. At the same time, from the top RHIC to the LHC energies, a nearly invariant  $T_0$  reflects the limiting deposition of collision energy. Comparing with peripheral collisions, the slight larger or nearly the same  $\beta_T$  in central collisions renders similar expansion in both the centralities. At the same time, at the top RHIC and the LHC energies, the two systems also show similar expansion due to similar  $\beta_T$ .

It should be noted that, although Eq. (2) [14] does not implement the azimuthal integral over the freeze-out surface which gives rise to the modified Bessel functions in Eq. (1), it does not affect the extractions of kinetic freeze-out parameters due to the application of numerical integral. Although Eq. (3) [15, 16] assumes a single, infinitesimally thin shell of fixed flow velocity and also does not perform the integral over the freeze-out surface, it can extract the mean trend of kinetic freeze-out parameters. As for the alternative method [12, 17–20, 22–24], it assumes non-relativistic flow velocities in the expressions used to extract the freeze-out parameters, which is the case that  $\beta_T$  is indeed not too large at the top RHIC and LHC energies.

## 4 Conclusions

We summarize here our main observations and conclusions.

(a) The  $p_T$  spectra of  $\pi^\pm$ ,  $K^\pm$ ,  $K_S^0$ ,  $p$ , and  $\bar{p}$  produced in central (0–5% and 0–12%) and peripheral (80–92% and 60–80%) Au-Au collisions at  $\sqrt{s_{NN}} = 200$  GeV and in central (0–5%) and peripheral (80–90% and 60–80%) Pb-Pb collisions at  $\sqrt{s_{NN}} = 2.76$  TeV have been analyzed by a few different superpositions in which the distributions related to the extractions of  $T_0$  and  $\beta_T$  are used for the soft component and the inverse power law is used for the hard component. We have used five distributions, i) the Blast-Wave model with Boltzmann-Gibbs statistics, ii) the Blast-Wave model with Tsallis statistics, iii) the Tsallis distribution with flow effect,

iv)<sub>a</sub> the Boltzmann distribution, and iv)<sub>b</sub> the Tsallis distribution, for the soft component. The first three distributions are in fact three methods for the extractions of  $T_0$  and  $\beta_T$ . The last two distributions are used in the fourth method, i.e. the alternative method.

(b) The experimental data measured by the PHENIX, STAR, and ALICE Collaborations are fitted by the model results. Our calculations show that the parameter  $T_0$  obtained by the method i) with the conventional treatment for central collisions is smaller than that for peripheral collisions, which is inconsistent with the results obtained by other model methods. In the conventional treatment, the parameter  $\beta_T$  in peripheral collisions is taken to be nearly zero, which results in a larger  $T_0$  than normal case. By using the conventional treatment, both the methods i) and ii) show a nearly zero  $\beta_T$  in peripheral collisions according to refs. [11, 14], while other methods show a considerable  $\beta_T$  in both central and peripheral collisions.

(c) In central and peripheral collisions, we have to select a suitable  $\beta_T$  so that we can determine which  $T_0$  is larger. We are inclined to use a non-zero  $\beta_T$  for peripheral collisions due to small system also showing collective expansion. We have given a re-examination for  $\beta_T$  in peripheral collisions in the methods i) and ii) in which  $\beta_T$  is taken to be  $\sim (0.40 \pm 0.07)c$ . By using a non-zero  $\beta_T$ , the first two methods show approximately consistent results with other methods, not only for  $T_0$  but also for  $\beta_T$ , though the method iii) gives a larger  $\beta_T$ . We have uniformly obtained a larger  $T_0$  in central collisions by the four methods. In particular, the parameter  $T_0$  at the LHC is larger than or equal to that at the RHIC. Except the method iii), other methods show a slightly larger or nearly invariant  $\beta_T$  in central collisions comparing with peripheral collisions, and at the LHC comparing with the RHIC.

(d) The new results obtained by the widely used Blast-Wave model with Boltzmann-Gibbs or Tsallis statistics are in agreement with those obtained by the newly used alternative method which uses the Boltzmann or Tsallis distribution. This consistency confirms the validity of the alternative method. The result that the central collisions have a larger  $T_0$  renders more deposition of collision energy and higher excitation of interacting system due to more participant nucleons taking part in the violent collisions. From the RHIC to LHC, the slightly increased or nearly invariant  $T_0$  renders the limiting or maximum deposition of colli-

sions energy. From central to peripheral collisions and from the RHIC to LHC, the slightly increased or nearly invariant  $\beta_T$  renders the limiting or maximum blast of interacting system.

### Conflict of Interests

The authors declare that there is no conflict of interests regarding the publication of this paper.

### Acknowledgments

This work was supported by the National Natural Science Foundation of China under Grant Nos. 11575103 and 11747319, the Shanxi Provincial Natural Science Foundation under Grant No. 201701D121005, and the Fund for Shanxi “1331 Project” Key Subjects Construction.

## References

- [1] N. Xu (for the STAR Collaboration), An overview of STAR experimental results. *Nucl. Phys. A* **931**, 1 (2014). doi: 10.1016/j.nuclphysa.2014.10.022
- [2] S. Chatterjee, S. Das, L. Kumar, D. Mishra, B. Mohanty, R. Sahoo, N. Sharma, Freeze-out parameters in heavy-ion collisions at AGS, SPS, RHIC, and LHC energies. *Adv. High Energy Phys.* **2015**, 349013 (2015). doi: 10.1155/2015/349013
- [3] S. Chatterjee, B. Mohanty, R. Singh, Freezeout hypersurface at energies available at the CERN Large Hadron Collider from particle spectra: Flavor and centrality dependence. *Phys. Rev. C* **92**, 024917 (2015). doi: 10.1103/PhysRevC.92.024917
- [4] S. Chatterjee, B. Mohanty, Production of light nuclei in heavy-ion collisions within a multiple-freezeout scenario. *Phys. Rev. C* **90**, 034908 (2014). doi: 10.1103/PhysRevC.90.034908
- [5] S.S. Räsänen (for the ALICE Collaboration), ALICE overview. *EPJ Web Conf.* **126**, 02026 (2016). doi: 10.1051/epjconf/201612602026
- [6] M. Floris, Hadron yields and the phase diagram of strongly interacting matter. *Nucl. Phys. A* **931**, 103 (2014). doi: 10.1016/j.nuclphysa.2014.09.002
- [7] S. Das, D. Mishra, S. Chatterjee, B. Mohanty, Freeze-out conditions in proton-proton collisions at the highest energies available at the BNL Relativistic Heavy Ion Collider and the CERN Large Hadron Collider. *Phys. Rev. C* **95**, 014912 (2017). doi: 10.1103/PhysRevC.95.014912
- [8] P. Huovinen, Chemical freeze-out temperature in the hydrodynamical description of Au+Au collisions at

- $\sqrt{s_{NN}} = 200$  GeV. Eur. Phys. J. A **37**, 121 (2008). doi: 10.1140/epja/i2007-10611-3
- [9] B. De, Non-extensive statistics and understanding particle production and kinetic freeze-out process from  $p_T$ -spectra at 2.76 TeV. Eur. Phys. J. A **50**, 138 (2014). doi: 10.1140/epja/i2014-14138-2
- [10] A. Andronic, An overview of the experimental study of quark-gluon matter in high-energy nucleus-nucleus collisions. Int. J. Mod. Phys. A **29**, 1430047 (2014). doi: 10.1142/S0217751X14300476
- [11] E. Schnedermann, J. Sollfrank, U. Heinz, Thermal phenomenology of hadrons from 200A GeV S+S collisions. Phys. Rev. C **48**, 2462 (1993). doi: 10.1103/PhysRevC.48.2462
- [12] B. I. Abelev *et al.* (STAR Collaboration), Systematic measurements of identified particle spectra in pp, d+Au, and Au+Au collisions at the STAR detector. Phys. Rev. C **79**, 034909 (2009). doi: 10.1103/PhysRevC.79.034909
- [13] B. I. Abelev *et al.* (STAR Collaboration), Identified particle production, azimuthal anisotropy, and interferometry measurements in Au+Au collisions at  $\sqrt{s_{NN}} = 9.2$  GeV. Phys. Rev. C **81**, 024911 (2010). doi: 10.1103/PhysRevC.81.024911
- [14] Z.B. Tang, Y.C. Xu, L.J. Ruan, G. van Buren, F.Q. Wang, Z.B. Xu, Spectra and radial flow in relativistic heavy ion collisions with Tsallis statistics in a blast-wave description. Phys. Rev. C **79**, 051901(R) (2009). doi: 10.1103/PhysRevC.79.051901
- [15] T. Bhattacharyya, J. Cleymans, A. Khuntia, P. Pareek, R. Sahoo, Radial flow in non-extensive thermodynamics and study of particle spectra at LHC in the limit of small ( $q - 1$ ). Eur. Phys. J. A **52**, 30 (2016). doi: 10.1140/epja/i2016-16030-5
- [16] D. Thakur, S. Tripathy, P. Garg, R. Sahoo, J. Cleymans, Indication of a differential freeze-out in proton-proton and heavy-ion collisions at RHIC and LHC energies. Adv. High Energy Phys. **2016**, 4149352 (2016). doi: 10.1155/2016/4149352
- [17] S. Takeuchi, K. Murase, T. Hirano, P. Huovinen, Y. Nara, Effects of hadronic rescattering on multistrange hadrons in high-energy nuclear collisions. Phys. Rev. C **92**, 044907 (2015). doi: 10.1103/PhysRevC.92.044907
- [18] H. Heiselberg, A.-M. Levy, Elliptic flow and Hanbury-Brown-Twiss correlations in noncentral nuclear collisions. Phys. Rev. C **59**, 2716 (1999). doi: 10.1103/PhysRevC.59.2716
- [19] U. W. Heinz, Lecture Notes for lectures presented at the 2nd CERN-Latin-American School of High-Energy Physics, June 1-14, 2003, San Miguel Regla, Mexico, arXiv:hep-ph/0407360 (2004).
- [20] R. Russo, Measurement of  $D^+$  meson production in p-Pb collisions with the ALICE detector, PhD Thesis, Universita degli Studi di Torino, Italy, arXiv:1511.04380 [nucl-ex] (2015).
- [21] F.-H. Liu, Y.-Q. Gao, H.-R. Wei, On descriptions of particle transverse momentum spectra in high energy collisions. Adv. High Energy Phys. **2014**, 293873 (2014). doi: 10.1155/2014/293873
- [22] H.-R. Wei, F.-H. Liu, R.A. Lacey, Kinetic freeze-out temperature and flow velocity extracted from transverse momentum spectra of final-state light flavor particles produced in collisions at RHIC and LHC. Eur. Phys. J. A **52**, 102 (2016). doi: 10.1140/epja/i2016-16102-6
- [23] H.-L. Lao, H.-R. Wei, F.-H. Liu, R.A. Lacey, An evidence of mass-dependent differential kinetic freeze-out scenario observed in Pb-Pb collisions at 2.76 TeV. Eur. Phys. J. A **52**, 203 (2016). doi: 10.1140/epja/i2016-16203-2
- [24] H.-R. Wei, F.-H. Liu, R.A. Lacey, Disentangling random thermal motion of particles and collective expansion of source from transverse momentum spectra in high energy collisions. J. Phys. G **43**, 125102 (2016). doi: 10.1088/0954-3899/43/12/125102
- [25] S. S. Adler *et al.* (PHENIX Collaboration), Identified charged particle spectra and yields in Au+Au collisions at  $\sqrt{s_{NN}} = 200$  GeV. Phys. Rev. C **69**, 034909 (2004). doi: 10.1103/PhysRevC.69.034909
- [26] B. I. Abelev *et al.* (STAR Collaboration), Identified baryon and meson distributions at large transverse momenta from Au+Au collisions at  $\sqrt{s_{NN}} = 200$  GeV. Phys. Rev. Lett. **97**, 152301 (2006). doi: 10.1103/PhysRevLett.97.152301
- [27] G. Agakishiev *et al.* (STAR Collaboration), Identified hadron compositions in  $p + p$  and Au+Au collisions at high transverse momenta at  $\sqrt{s_{NN}} = 200$  GeV. Phys. Rev. Lett. **108**, 072302 (2012). doi: 10.1103/PhysRevLett.108.072302
- [28] B. Abelev *et al.* (ALICE Collaboration), Centrality dependence of  $\pi$ ,  $K$ , and  $p$  in Pb-Pb collisions at  $\sqrt{s_{NN}} = 2.76$  TeV. Phys. Rev. C **88**, 044910 (2013). doi: 10.1103/PhysRevC.88.044910
- [29] J. Adam *et al.* (ALICE Collaboration), Centrality dependence of the nuclear modification factor of charged pions, kaons, and protons in Pb-Pb collisions at  $\sqrt{s_{NN}} = 2.76$  TeV. Phys. Rev. C **93**, 034913 (2016). doi: 10.1103/PhysRevC.93.034913
- [30] E. Schnedermann, U. Heinz, Relativistic hydrodynamics in a global fashion. Phys. Rev. C **47**, 1738 (1993). doi: 10.1103/PhysRevC.47.1738
- [31] L. Kumar (for the STAR Collaboration), Systematics of kinetic freeze-out properties in high energy collisions from STAR. Nucl. Phys. A **931**, 1114 (2014). doi: 10.1016/j.nuclphysa.2014.08.085
- [32] H. Zheng, L.L. Zhu, Comparing the Tsallis distribution with and without thermodynamical description in

- $p+p$  collisions. *Adv. High Energy Phys.* **2016**, 9632126 (2016). doi: 10.1155/2016/9632126
- [33] J. Cleymans, D. Worku, Relativistic thermodynamics: Transverse momentum distributions in high-energy physics. *Eur. Phys. J. A* **48**, 160 (2012). doi: 10.1140/epja/i2012-12160-0
- [34] R. Odorico, Does a transverse energy trigger actually trigger on large- $p_T$  jets? *Phys. Lett. B* **118**, 151 (1982). doi: 10.1016/0370-2693(82)90620-7
- [35] G. Arnison *et al.* (UA1 Collaboration), Transverse momentum spectra for charged particles at the CERN proton-antiproton collider. *Phys. Lett. B* **118**, 167 (1982). doi: 10.1016/0370-2693(82)90623-2
- [36] T. Mizoguchi, M. Biyajima, N. Suzuki, Analyses of whole transverse momentum distributions in  $p\bar{p}$  and  $pp$  collisions by using a modified version of Hagedorn's formula. *Int. J. Mod. Phys. A* **32**, 1750057 (2017). doi: 10.1142/S0217751X17500579
- [37] H.-L. Lao, F.-H. Liu, R.A. Lacey, Extracting kinetic freeze-out temperature and radial flow velocity from an improved Tsallis distribution. *Eur. Phys. J. A* **53**, 44 (2017). doi: 10.1140/epja/i2017-12238-1; and Erratum. *Eur. Phys. J. A* **53**, 143 (2017). doi: 10.1140/epja/i2017-12333-3
- [38] F.-H. Liu, Y.-Q. Gao, B.-C. Li, Comparing two-Boltzmann distribution and Tsallis statistics of particle transverse momentums in collisions at LHC energies. *Eur. Phys. J. A* **50**, 123 (2014). doi: 10.1140/epja/i2014-14123-9
- [39] H. Zheng, L.L. Zhu, Can Tsallis distribution fit all the particle spectra produced at RHIC and LHC? *Adv. High Energy Phys.* **2015**, 180491 (2015). doi: 10.1155/2015/180491
- [40] H.C. Song, Y. Zhou, K. Gajdošová, Collective flow and hydrodynamics in large and small systems at the LHC. *Nucl. Sci. Tech.* **28**, 99 (2017). doi: 10.1007/s41365-017-0245-4